LETTER

Very large release of mostly volcanic carbon during the Palaeocene–Eocene Thermal Maximum

Marcus Gutjahr[1,2], Andy Ridgwell[3,4], Philip F. Sexton[5], Eleni Anagnostou[1], Paul N. Pearson[6], Heiko Pälike[7], Richard D. Norris[8], Ellen Thomas[9,10] & Gavin L. Foster[1]

The Palaeocene–Eocene Thermal Maximum[1,2] (PETM) was a global warming event that occurred about 56 million years ago, and is commonly thought to have been driven primarily by the destabilization of carbon from surface sedimentary reservoirs such as methane hydrates[3]. However, it remains controversial whether such reservoirs were indeed the source of the carbon that drove the warming[1,3–5]. Resolving this issue is key to understanding the proximal cause of the warming, and to quantifying the roles of triggers versus feedbacks. Here we present boron isotope data—a proxy for seawater pH—that show that the ocean surface pH was persistently low during the PETM. We combine our pH data with a paired carbon isotope record in an Earth system model in order to reconstruct the unfolding carbon-cycle dynamics during the event[6,7]. We find strong evidence for a much larger (more than 10,000 petagrams)—and, on average, isotopically heavier—carbon source than considered previously[8,9]. This leads us to identify volcanism associated with the North Atlantic Igneous Province[10,11], rather than carbon from a surface reservoir, as the main driver of the PETM. This finding implies that climate-driven amplification of organic carbon feedbacks probably played only a minor part in driving the event. However, we find that enhanced burial of organic matter seems to have been important in eventually sequestering the released carbon and accelerating the recovery of the Earth system[12].

In attempting to understand the effects of massive carbon release on the Earth system, arguably the greatest uncertainties (aside from climate[13] and ecological sensitivities[14]) concern the role of carbon-cycle feedbacks[15]. A past event that could shed light on such feedbacks is the PETM[1]—a transient surface warming of 4–5 °C (ref. 2), associated with ecological disruption, that occurred around 55.8 million years ago[16]. Estimates of the total amount of carbon released during the PETM vary from around 3,000 Pg to more than 10,000 Pg (refs 7, 8); these estimates span the range of present-day fossil-fuel reserves[17], but also reflect considerable uncertainty. The sources of the carbon released during the PETM are also highly uncertain, and have been proposed to include methane hydrates[3], permafrost[4] and marine sedimentary[5] organic matter. To further complicate the matter, proposed triggers for the PETM include variations in Earth's orbit[4] and an extraterrestrial impact[18]. Another possible carbon source is the massive flood basalts and sill emplacement occurring around the time of the PETM and associated with the North Atlantic Igneous Province (NAIP)[10,11,19], but this source is not linked to a feedback with climate. If we are to fully understand the palaeo-record—and to exploit it in order to improve our understanding of the longer-term consequences of anthropogenic carbon emissions—we must resolve the balance of carbon sources that gave rise to the PETM, and thereby deconvolve the roles of triggers versus feedbacks. To provide fresh insight into the amount and sources of carbon involved in PETM warming, we present here new, paired, ocean surface boron isotope data (a well established proxy for ambient surface seawater pH[20,21]) and carbon isotope data. We use these records simultaneously to constrain the time-varying sources and sinks of carbon across the PETM in a data-assimilation approach using an Earth system model.

We generated near-continuous boron, oxygen and carbon isotope records from buried fossils of the extinct, mixed-layer-dwelling foraminifer *Morozovella subbotinae*, found at Deep Sea Drilling Project (DSDP) Site 401 in the northeast Atlantic Ocean (at 47° 25.65′ N, 08° 48.62′ W) (Fig. 1). One characteristic signature of PETM sections is a negative carbon isotope excursion (CIE), found both in marine and terrestrial sediments[1]. We sampled the sediment sequence over an interval corresponding to around 300 kyr before the CIE to about 500 kyr afterwards, using a new stratigraphy for Site 401 (see Methods). To avoid alignment issues between proxies, we measured boron, oxygen and carbon isotopic compositions as well as elemental compositions on the same samples (Fig. 1a, c, e and Extended Data Figs 1, 2).

Our measured CIE magnitude at Site 401 of -3.4‰ (Fig. 1a) is at the upper end of planktic foraminiferal $\delta^{13}C$ records (minimum CIE, -0.7‰; maximum, -4.4‰; average, -2.7‰; $n = 36$)[1], suggesting that our sampling encompasses close to the full magnitude of the CIE (see Methods). The CIE is accompanied by a decrease in $\delta^{11}B$ of almost 1.7‰ (Fig. 1c). The lowest $\delta^{13}C$ and $\delta^{11}B$ values are both observed about 25 kyr after the onset of the CIE in our preferred age model, giving an inferred duration for the onset phase of the CIE that agrees well with an independently dated record from Spitsbergen[16].

Because there are uncertainties in the boron isotopic composition of seawater ($\delta^{11}B_{sw}$) prior to the PETM, we tie our initial, pre-CIE boron-isotope-derived pH to surface ocean pH (7.75), as simulated by the cGENIE Earth system model[6] and following the approach of a previous PETM model–data pH study[20]. Our $\delta^{11}B$ measurements then dictate the timing and magnitude of how surface ocean pH deviated from this value during the PETM. In our pH reconstruction, we calculate an uncertainty envelope that accounts for uncertainties in surface ocean temperature and salinity and for $\delta^{11}B$ measurement errors, and test two contrasting end-member $\delta^{11}B$–pH calibrations for *M. subbotinae* (see Methods). We focus on the $\delta^{11}B_{foram} = \delta^{11}B_{borate}$ calibration, giving an estimated $\delta^{11}B_{sw}$ (38.9‰ ± 0.4‰) that is consistent with a recent reconstruction of Eocene $\delta^{11}B_{sw}$ based on $\delta^{11}B$ (ref. 21).

We find that the evolution of ocean pH across the PETM is characterized by a negative excursion of 0.27 (range 0.18–0.41) or 0.36 (0.21–0.56) pH units, depending on which $\delta^{11}B$–pH calibration is used (Fig. 2 and Extended Data Fig. 3a), and in general agreement with a recently published PETM $\delta^{11}B$ record[20] (Fig. 2). The wide

[1]Ocean and Earth Science, National Oceanography Centre Southampton, University of Southampton, Southampton SO17 1BJ, UK. [2]GEOMAR Helmholtz Centre for Ocean Research Kiel, Wischhofstrasse 1–3, 24148 Kiel, Germany. [3]School of Geographical Sciences, Bristol University, Bristol BS8 1SS, UK. [4]Department of Earth Sciences, University of California at Riverside, Riverside, California 92521, USA. [5]School of Environment, Earth and Ecosystem Sciences, The Open University, Milton Keynes MK7 6AA, UK. [6]School of Earth and Ocean Sciences, Cardiff University, Cardiff CF10 3AT, UK. [7]MARUM, Center for Marine Environmental Sciences, University of Bremen, 28359 Bremen, Germany. [8]Scripps Institution of Oceanography, University of California, San Diego, La Jolla, California 92037, USA. [9]Department of Geology and Geophysics, Yale University, New Haven, Connecticut 06520, USA. [10]Department of Earth and Environmental Sciences, Wesleyan University, Middletown, Connecticut 06459, USA.
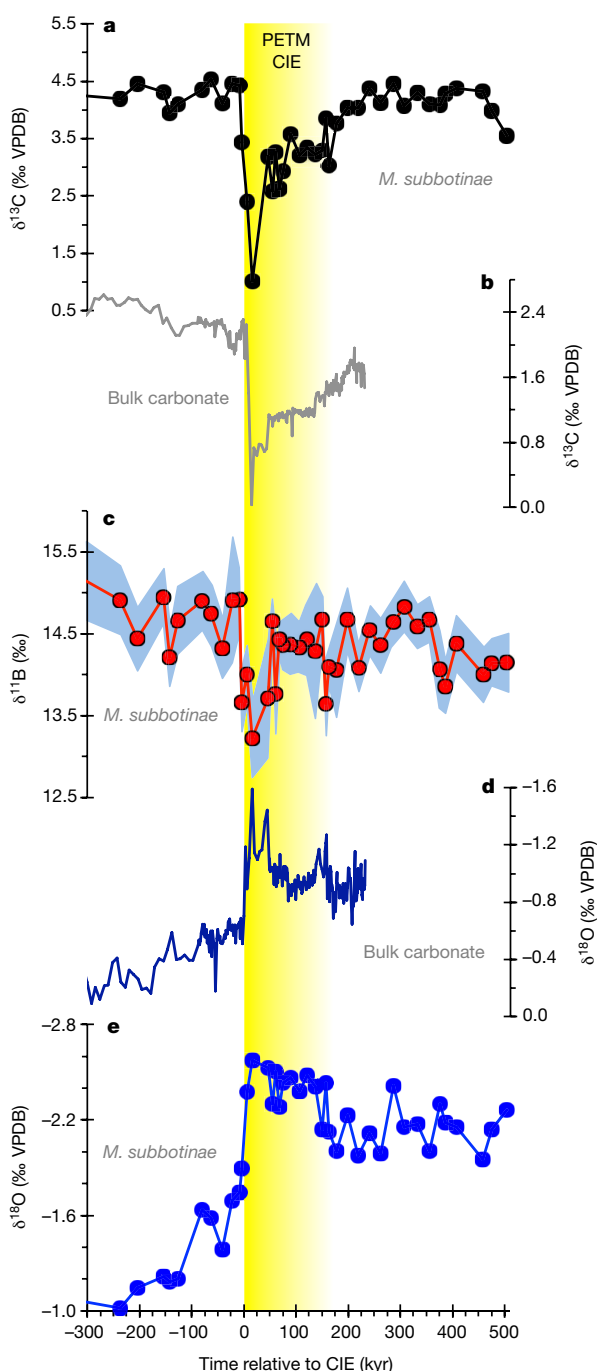
Figure 1 | Stable-isotope data from DSDP Site 401. a–e, $\delta^{13}C$ records for foraminifera (*M. subbotinae*; **a**) and bulk carbonate (**b**); $\delta^{11}B$ records for foraminifera, including analytical 2 s.d. uncertainties (blue shaded band; **c**); and $\delta^{18}O$ records for bulk carbonate (**d**) and foraminifera (**e**), plotted relative to the onset of the PETM carbon isotope excursion (CIE; yellow bar). These records were obtained from DSDP Site 401 (47° 25.65′ N, 08° 48.62′ W; 2,495 m) using our preferred age model (see Methods). VPDB is the Vienna Pee Dee Belemnite carbon isotope standard.

geographic distribution (covering the Pacific Ocean and the south and north Atlantic Ocean), but close correspondence in magnitude, of all PETM $\delta^{11}B$–pH records generated to date gives us confidence that a global surface pH excursion signal is captured at DSDP Site 401. The fact that ocean surface pH responds relatively uniformly in models[14] supports the evidence from multiple $\delta^{11}B$ records (Fig. 2)

that a single, open-ocean site can be representative of the global trend (see Methods).

To reconstruct PETM carbon release and its average isotopic composition, we devised a new data-assimilation methodology. We built on previous work[7] in which a single $\delta^{13}C$ record was assimilated ('inverted') to constrain the time-varying addition of carbon, but exploited a more direct indicator of carbon addition—ocean surface pH (Fig. 2). This allows our $\delta^{13}C$ record simultaneously to provide a second, independent constraint on the isotopic composition of the carbon emissions in a transient, 500-kyr assimilation of both records (see Methods). We explored a wide range of different model parameterizations and proxy assumptions (Extended Data Table 1a), but focus here on the results of the data assimilation of the smoothed record.

Using our preferred age model (R07sm; Extended Data Table 1a), we diagnose a cumulative PETM carbon release that reaches about 10,200 Pg, with almost all emissions occurring in the first 50 kyr (Fig. 3d). This estimate is largely independent of the choice of age model (Extended Data Table 1), which primarily affects the cumulative carbon emissions associated with the onset interval itself (which we define as the period from the first trace of $\delta^{13}C$ decline in our records up to peak CIE values), rather than the total emissions associated with the event as a whole. We demonstrate this in idealized model experiments (Extended Data Fig. 5 and Extended Data Table 1b), in which we find that total carbon emissions over 50 kyr are essentially independent of the assumed duration of the onset interval, and vary by only ±20% at the 20-kyr horizon. Thus, it is the extended duration of low pH across the PETM as a whole and the existence of the so-called carbon-isotope plateau[2]—rather than the duration of the onset interval alone—that lead to our diagnosis of total PETM emissions of the order of 10,000 Pg. Uncertainty in the duration of low pH equates to about 100 Pg of carbon per kyr at the 50-kyr horizon (Extended Data Fig. 5), consistent with the total carbon emissions of around 12,000 Pg that we deduced for our alternative age model, which has an extended duration of low pH (Extended Data Fig. 3c).

In response to carbon emissions during the PETM, the atmospheric partial pressure of CO_2 in our model increases from about 866 µatm to a peak value of 2,176 µatm (range 1,507–4,080 µatm), consistent with an independent study of atmospheric CO_2 partial pressures that was based on variable terrestrial and marine $\delta^{13}C$ gradients during the PETM[22]. We find that the corresponding projected annual mean sea surface temperature (SST) increase is 3.6 °C—close to the observation-based global mean warming estimate of 4–5 °C (ref. 2). We also find that, in response to carbon emissions (and surface ocean pH suppression), there is a shoaling of the carbonate compensation depth (CCD) in the model (the depth horizon below which calcium carbonate is not preserved[23]) (Extended Data Fig. 7). In previous global carbon-cycle model analyses of the PETM, the CCD has been used as a data constraint, leading to the conclusion that carbon emissions of the order of 10,000 Pg are too high[8]. In contrast, in our model, the relatively long (more than 50 kyr) duration of low ocean pH conditions (Fig. 3), in conjunction with weathering feedbacks, leads to a partial decoupling of pH and ocean carbonate saturation[24]—and hence to a relatively muted response of the CCD, despite the large emissions (Extended Data Fig. 7 and Methods).

We further find that carbon emission rates during the PETM peak at 0.58 Pg of carbon per year (Fig. 3c and Extended Data Table 1a), although we assign rather less confidence to these, because their value is sensitive to the duration of the onset of the PETM and hence to the specific age model (Extended Data Table 1a). To put this in perspective, for PETM carbon emission rates to approach those generated currently from fossil fuels (around 10 Pg of carbon per year; ref. 17), the PETM onset would have to have occurred over a period of 200 to 500 years—a duration not supported by any independent age model[7,16,24,25]. The fact that the peak carbon emission rate during the PETM was much lower than the present-day rate suggests that any impacts on ocean acidification (especially in terms of carbonate saturation) should have
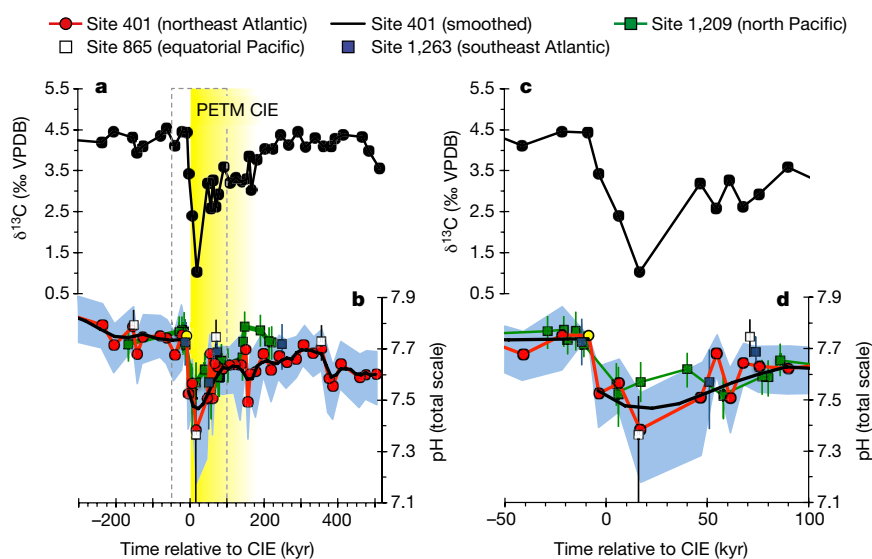
Figure 2 | $\delta^{13}C$ evolution and pH reconstruction based on analysis of boron isotopes in *M. subbotinae* from Site 401. a, b, The entire record; **c, d**, the CIE interval (dotted grey outline in **a, b**). Also shown are data from ref. 20 (for Sites 865, 1,209 and 1,263) on the original age model, with pH values recalculated using a laboratory offset such that the pre-PETM

pH calculated using our Monte Carlo approach at Site 1,209 is 7.74, given the distribution of seawater $\delta^{11}B$ determined at Site 401 (38.9‰ ± 0.4‰). This resulted in a mean correction of the literature data[20] of −0.32‰. The blue shaded band in **b** and **d** illustrates $\delta^{11}B$-based pH uncertainties (2 s.d.).

been much lower during the PETM than they will be in the future[6,15]. However, we cannot rule out the possibility that multiple, short-lived pulses of carbon release (of more than 0.58 Pg per year) occurred throughout an extended (for example, 20 kyr) onset[24].

In addition to the emissions obtained by matching the pH decline, use of the $\delta^{13}C$ data as an independent constraint leads us to deduce a flux-weighted mean $\delta^{13}C$ of released carbon of −11‰ (Fig. 3f, l). However, the smoothed $\delta^{13}C$ record (−2.6‰ excursion) on which we focus probably underestimates the isotopic magnitude of the event. For instance, if the 'true' PETM CIE were as large as −4.0‰ (refs 7, 24) and we simply proportionally scaled the value of $\delta^{13}C_{input}$ diagnosed on the basis of a −2.6‰ excursion, we would obtain a more-depleted mean source of −17‰. Uncertainty in our ocean pH reconstruction also affects the diagnosed carbon-source composition. Our minimum pH decrease of 0.18 pH units requires only 5,700 Pg of carbon, with a mean $\delta^{13}C_{input}$ of −19‰. However, the comparatively muted surface warming seen in this 'minimal pH change' model experiment (2.25 °C of warming; Extended Data Table 1a, experiment R07am_HI) is difficult to reconcile with the observed warming of 4–5 °C (ref. 2) Conversely, the upper end of our measured pH increase would require the emission of considerably more carbon (19,960 Pg) with a correspondingly heavier carbon-isotopic composition of −6.6‰ (Extended Data Table 1a).

Our diagnosed carbon input over the event probably reflects a combination of carbon sources; for instance, a mean of −11‰ could reflect a 75% contribution of mantle-derived carbon (with $\delta^{13}C_{source}$ being about −6‰) plus a 25% contribution from permafrost (about −26‰), or 90% mantle-derived carbon plus 10% methane hydrates (about −60‰). In such scenarios, volcanism triggered the PETM, and thawing permafrost in Antarctica[4] or destabilization of methane hydrates provided amplifying feedback. Assuming a −4‰ magnitude excursion and a mean $\delta^{13}C_{input}$ of −17‰ still requires a substantial CO_2 contribution from volcanism[10], but would allow for the possibility of a greater role for organic-carbon feedbacks—almost 60% for organic matter or about 20% for methane hydrates.

Until now, the PETM has largely been viewed as an event that was dominated by feedbacks between the climate and carbon reservoirs[3]. Yet there is abundant evidence of an intimate link in time with the opening of the North Atlantic[11], with volcanism and ash deposition in the North Atlantic region occurring from immediately before the

onset of the PETM, as also recorded by declining $^{187}Os/^{188}Os$ ratios in sediments[19]. Radiometric dating places the PETM coincident with a roughly 1-million-year interval of massive flood basalt volcanism[11] and the emplacement of magmatic sills[26], both of which represent large carbon sources. Degassing CO_2 from magma yields an estimated carbon emission of 3,600–6,000 g per m³ (ref. 27), and combining this with the estimated volume of the NAIP as a whole (5×10^6 km³ to 10×10^6 km³; refs 11, 27) results in a potential carbon source of 18,000 Pg to 60,000 Pg. The interaction of magmatism with organic-rich sediments could enhance carbon release via thermogenic methane production[10,11], which is estimated to generate from 3,000–6,000 Pg of carbon[28] up to as much as 15,000 Pg (ref. 10). Available carbon reservoirs are thus more than sufficient to provide the 10,200–12,200 Pg required by our data assimilation, and we further note that an all-volcanic carbon-driver scenario for the PETM is possible if thermogenic methane[10,11] had provided the isotopically lighter end-member. On the other hand, NAIP magmatic activity took place over several million years[10,11], and it is not known how carbon emissions were distributed over this time interval. Nonetheless, dating, biostratigraphy and seismic constraints do, first, place an interval of volcanism in East Greenland[11] and of sill emplacement in the Vøring Basin (off Norway)[26] at the time of PETM onset; and second, identify hundreds of degassing structures consistent with thermogenic carbon release as forming close to the Palaeocene–Eocene boundary[10], with one structure constrained to have been active during the PETM itself[9]. Thus, release of a disproportionate amount of NAIP carbon during the PETM is consistent with available geological evidence and with our data-inferred modelling of carbon sources and total carbon release. More work is clearly needed, however, to date further specific volcanic episodes and to refine estimates of carbon reservoirs.

Our paired $\delta^{11}B$–$\delta^{13}C$ data also provide insights into how the climate system recovered after the PETM. Using cGENIE, we find that, once carbon emissions ceased (about 55 kyr after the PETM began; Fig. 3c), elevated global temperatures (Fig. 3a) and enhanced rates of silicate weathering (Fig. 3c) drove a trend of increasing ocean surface pH that closely followed the observed surface ocean pH recovery (Fig. 3b; see Methods). However, we also find a model–data misfit of up to about 1‰ in $\delta^{13}C$ during the recovery phase (Fig. 3e). We therefore performed another set of experiments in which, after peak CIE, organic
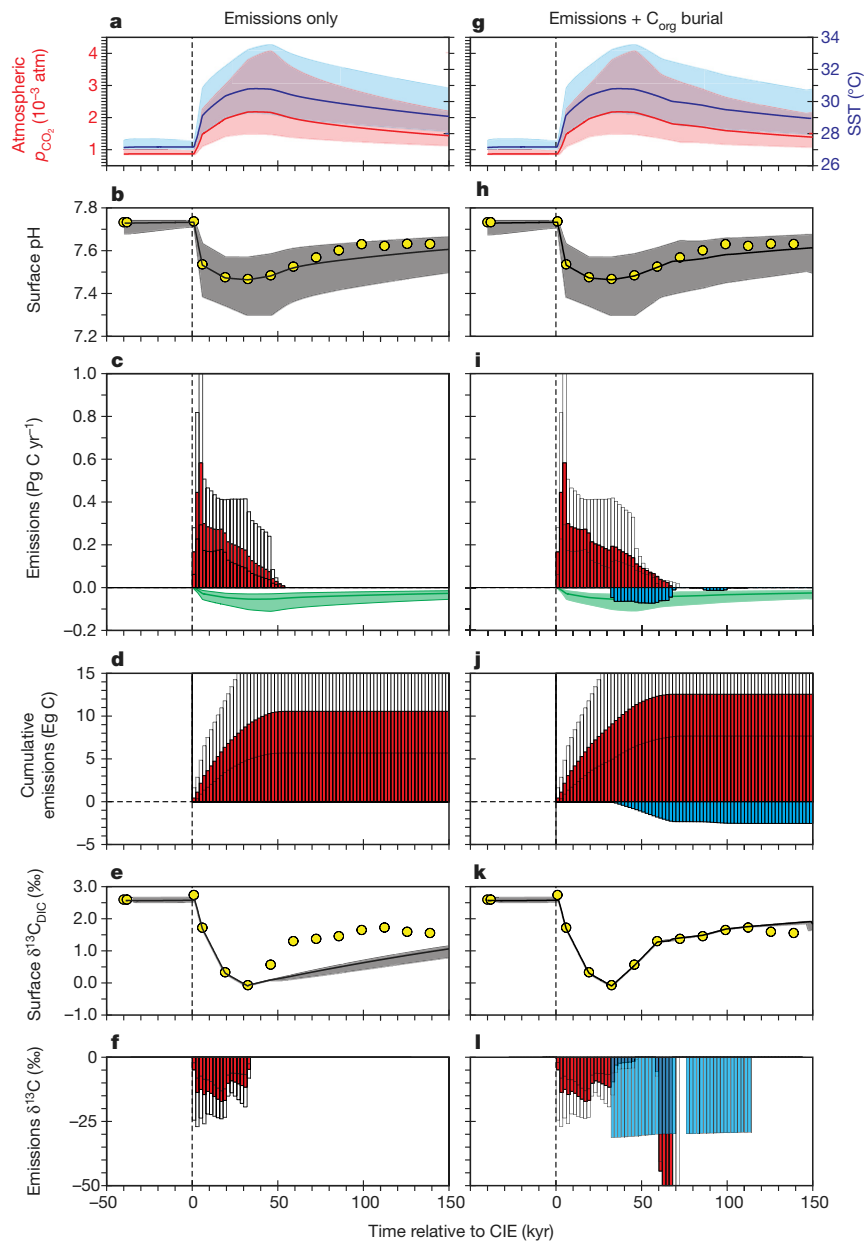
Figure 3 | Assimilation of data from our Earth system model. The left-hand panels show data from emissions-only experiments; the right-hand panels also account for the burial of organic carbon during recovery from the PETM. The vertical dotted lines show the time of onset of the PETM. **a, g**, Atmospheric partial CO_2 pressure (p_{CO_2}; red; left-hand axis) and mean global sea surface temperature (SST; blue; right-hand axis). **b, h**, Modelled mean global ocean surface pH (the yellow symbols denote the observed, smoothed, surface ocean pH data on the seawater scale). **c, i**, Model-diagnosed rates of CO_2 release (red) and excess CO_2

consumption due to silicate weathering (green) from PETM onset onwards. **d, j**, Cumulative CO_2 release (red) and organic carbon burial (blue). Eg, exagram (1×10^{18} g). **e, k**, Modelled mean global ocean surface $\delta^{13}C$ (observations are shown as yellow symbols). **f, l**, Model-diagnosed $\delta^{13}C$ from CO_2 release (red), and isotopic composition of buried carbon (blue). Shaded bands (**a, b, e, g, h, k**) and empty bars (**c, d, f, i, j, l**) reflect 95% uncertainty limits. Bars reflect 2-kyr averaging (**c, f, i, l**) or integration (**d, j**) bins. Model results are plotted from the onset of the CIE (0 kyr) onwards.

carbon (C_{org}) is removed from the ocean surface[29] and assumed to be buried whenever modelled mean ocean surface $\delta^{13}C$ registers lower-than-observed values (see Methods). These final results provide close agreement with the recovery trend in the $\delta^{13}C$ data (Fig. 3k), with a cumulative C_{org} burial (Fig. 3j, blue bars) of 2,500 Pg (at an average modelled marine value of −30.5‰), in agreement with other estimates (around 2,000 Pg carbon)[12] of the role of enhanced organic-matter burial in PETM recovery[29]. Enhanced C_{org} burial is also consistent with a reduction in deep-sea oxygenation[30].

These findings lead us to a view of the PETM as having been on the smaller end of a spectrum of severe perturbations of climate

and carbon cycling ('ocean anoxic events', or OAEs[30,31]) during the Cretaceous and Jurassic periods, despite it having been by far the largest end-member in a series of Paleocene–Eocene 'hyperthermal' events[32]. Our pH reconstruction, in conjunction with the observed $\delta^{13}C$ decline, suggests that the dominant carbon source during PETM onset had a comparatively heavy carbon isotope ratio, strongly implicating volcanism in triggering and driving the event. Our inferred mean $\delta^{13}C$ source of −11‰ to −17‰ is consistent with the isotopically relatively heavy source (about −15‰; ref. 33) inferred for the warming event at the end of the Permian period—suggesting mechanistic similarities between this and the PETM[27]. The implied important role for organic-

carbon deposition in the recovery after peak warming[12] represents another diagnostic feature of OAEs[31] (and of the end-Permian event). Arguably, the PETM will be of greatest value in further quantifying and understanding the precise role of feedbacks—those that amplify the initial CO_2 release and those that aid recovery from global warming—thereby helping researchers to reduce the uncertainties surrounding the response of the global carbon cycle and climate system to perturbation.

Online Content Methods, along with any additional Extended Data display items and Source Data, are available in the online version of the paper; references unique to these sections appear only in the online paper.

1. McInerney, F. A. & Wing, S. L. The Paleocene–Eocene Thermal Maximum: a perturbation of carbon cycle, climate, and biosphere with implications for the future. *Annu. Rev. Earth Planet. Sci.* **39,** 489–516 (2011).
2. Dunkley Jones, T. *et al.* Climate model and proxy data constraints on ocean warming across the Paleocene–Eocene Thermal Maximum. *Earth Sci. Rev.* **125,** 123–145 (2013).
3. Dickens, G. R., O'Neil, J. R., Rea, D. K. & Owen, R. M. Dissociation of oceanic methane hydrate as a cause of the carbon isotope excursion at the end of the Paleocene. *Paleoceanography* **10,** 965–971 (1995).
4. DeConto, R. M. *et al.* Past extreme warming events linked to massive carbon release from thawing permafrost. *Nature* **484,** 87–91 (2012).
5. Higgins, J. A. & Schrag, D. P. Beyond methane: towards a theory for the Paleocene–Eocene Thermal Maximum. *Earth Planet. Sci. Lett.* **245,** 523–537 (2006).
6. Ridgwell, A. & Schmidt, D. N. Past constraints on the vulnerability of marine calcifiers to massive carbon dioxide release. *Nat. Geosci.* **3,** 196–200 (2010).
7. Cui, Y. *et al.* Slow release of fossil carbon during the Palaeocene–Eocene Thermal Maximum. *Nat. Geosci.* **4,** 481–485 (2011).
8. Zeebe, R. E., Zachos, J. C. & Dickens, G. R. Carbon dioxide forcing alone insufficient to explain Palaeocene–Eocene Thermal Maximum warming. *Nat. Geosci.* **2,** 576–580 (2009).
9. Frieling, J. *et al.* Thermogenic methane release as a cause for the long duration of the PETM. *Proc. Natl Acad. Sci. USA* **113,** 12059–12064 (2016).
10. Svensen, H. *et al.* Release of methane from a volcanic basin as a mechanism for initial Eocene global warming. *Nature* **429,** 542–545 (2004).
11. Storey, M., Duncan, R. A. & Swisher, C. C. Paleocene–Eocene Thermal Maximum and the opening of the Northeast Atlantic. *Science* **316,** 587–589 (2007).
12. Bowen, G. J. & Zachos, J. C. Rapid carbon sequestration at the termination of the Palaeocene–Eocene Thermal Maximum. *Nat. Geosci.* **3,** 866–869 (2010).
13. Rohling, E. J. *et al.* Making sense of palaeoclimate sensitivity. *Nature* **491,** 683–691 (2012).
14. Gibbs, S. J. *et al.* Ocean warming, not acidification, controlled coccolithophore response during past greenhouse climate change. *Geology* **44,** 59–62 (2016).
15. Hönisch, B. *et al.* The geological record of ocean acidification. *Science* **335,** 1058–1063 (2012).
16. Charles, A. J. *et al.* Constraints on the numerical age of the Paleocene-Eocene boundary. *Geochem. Geophys. Geosyst.* **12,** Q0AA17 (2011).
17. Le Quéré, C. *et al.* Global carbon budget 2016. *Earth Syst. Sci. Data* **8,** 605–649 (2016).
18. Schaller, M. F., Fung, M. K., Wright, J. D., Katz, M. E. & Kent, D. V. Impact ejecta at the Paleocene–Eocene boundary. *Science* **354,** 225–229 (2016).
19. Wieczorek, R., Fantle, M. S., Kump, L. R. & Ravizza, G. Geochemical evidence for volcanic activity prior to and enhanced terrestrial weathering during the Paleocene Eocene Thermal Maximum. *Geochim. Cosmochim. Acta* **119,** 391–410 (2013).
20. Penman, D. E., Hönisch, B., Zeebe, R. E., Thomas, E. & Zachos, J. C. Rapid and sustained surface ocean acidification during the Paleocene–Eocene Thermal Maximum. *Paleoceanography* **29,** 357–369 (2014).
21. Anagnostou, E. *et al.* Changing atmospheric CO_2 concentration was the primary driver of early Cenozoic climate. *Nature* **533,** 380–384 (2016).
22. Schubert, B. A. & Jahren, A. H. Reconciliation of marine and terrestrial carbon isotope excursions based on changing atmospheric CO_2 levels. *Nat. Commun.* **4,** 1653 (2013).
23. Penman, D. E. *et al.* An abyssal carbonate compensation depth overshoot in the aftermath of the Palaeocene–Eocene Thermal Maximum. *Nat. Geosci.* **9,** 575–580 (2016).
24. Turner, S. K. & Ridgwell, A. Development of a novel empirical framework for interpreting geological carbon isotope excursions, with implications for the rate of carbon injection across the PETM. *Earth Planet. Sci. Lett.* **435,** 1–13 (2016).
25. Röhl, U., Westerhold, T., Bralower, T. J. & Zachos, J. C. On the duration of the Paleocene–Eocene thermal maximum (PETM). *Geochem. Geophys. Geosyst.* **8,** Q12002 (2007).
26. Svensen, H., Planke, S. & Corfu, F. Zircon dating ties NE Atlantic sill emplacement to initial Eocene global warming. *J. Geol. Soc. Lond.* **167,** 433–436 (2010).
27. Saunders, A. D. Two LIPs and two Earth-system crises: the impact of the North Atlantic Igneous Province and the Siberian Traps on the Earth-surface carbon cycle. *Geol. Mag.* **153,** 201–222 (2016).
28. Rampino, M. R. Peraluminous igneous rocks as an indicator of thermogenic methane release from the North Atlantic Volcanic Province at the time of the Paleocene–Eocene Thermal Maximum (PETM). *Bull. Volcanol.* **75,** 1–5 (2013).
29. Ma, Z. *et al.* Carbon sequestration during the Palaeocene–Eocene Thermal Maximum by an efficient biological pump. *Nat. Geosci.* **7,** 382–388 (2014).
30. Dickson, A. J., Cohen, A. S. & Coe, A. L. Seawater oxygenation during the Paleocene–Eocene Thermal Maximum. *Geology* **40,** 639–642 (2012).
31. Jenkyns, H. C. Cretaceous anoxic events—from continents to oceans. *J. Geol. Soc. Lond.* **137,** 171–188 (1980).
32. Turner, S. K., Sexton, P. F., Charles, C. D. & Norris, R. D. Persistence of carbon release events through the peak of early Eocene global warmth. *Nat. Geosci.* **7,** 748–751 (2014).
33. Payne, J. L. *et al.* Calcium isotope constraints on the end-Permian mass extinction. *Proc. Natl Acad. Sci. USA* **107,** 8543–8548 (2010).

METHODS

Site and sample selection. We selected DSDP Site 401, in the open northeast Atlantic Ocean (47° 25.65′ N, 08° 48.62′ W, 2,495 metres), for this study. The depth of the ocean at this site during the PETM was approximately 2,000 metres (ref. 34). We picked around 2 mg of the 250–300-μm size fraction of the mixed-layer dweller *M. subbotinae* for carbon, oxygen and boron isotopic analyses. We also carried out very-high-resolution $\delta^{18}O$ and $\delta^{13}C$ analyses of bulk carbonate over the studied interval, to establish a revised age model for Site 401. Planktic foraminifera are extremely well preserved at this site[35]; they are free from infilling and, particularly from the onset of the CIE upwards, are semi-glassy in appearance[36].

Sample treatment. Using a binocular microscope, we cracked open the picked foraminifera under glass plates, and then homogenized the sample, before splitting it into a fraction for stable-isotope ($\delta^{18}O$ and $\delta^{13}C$) analysis and another for the boron isotopic and elemental analyses (with a ratio of around 10/90). Purification and measurement of the boron fraction followed established protocols[37,38]. Samples were thoroughly cleaned to remove any adhering clays, and then oxidatively cleaned using buffered peroxide in a warm water bath, closely following the procedures in ref. 39. Boron isotopic and elemental analyses were carried out on a Thermo Scientific Neptune multicollector inductively coupled plasma mass spectrometer (MC-ICPMS) and an Element XR ICPMS, respectively, at the University of Southampton. Sample purification and handling was done in low-boron clean labs at the University of Southampton. The average boron total procedural blank was of the order of 30–50 pg ($n > 10$) and is hence negligible given our typical sample size (about 5–15 ng boron). Boron isotopic uncertainties are reported at the 2σ level, calculated using repeats of in-house carbonate standards[40]. Boron isotopic and elemental aliquots were measured using additional ammonia gas for better sample washout between samples, and strictly monitored during every analytical session[37]. Prior to analysis for boron isotopic composition, samples were screened for chemical consistency by checking various elemental ratios (B/Ca, Mg/Ca and Al/Ca; Extended Data Fig. 1). A few samples had elevated Al/Ca ratios (up to about 3,400 μmol per mol), but this feature did not translate into altered $\delta^{11}B$ values (Extended Data Fig. 1).

Carbon and oxygen isotope aliquots were measured on a Thermo Finnigan MAT252 stable-isotope mass spectrometer at the GEOMAR Helmholtz Centre for Ocean Research. Additionally, some foraminifera-based $\delta^{18}O$ and $\delta^{13}C$ analyses, as well as all bulk carbonate stable-isotope measurements, were carried out at MARUM Bremen on a Finnigan 251 gas isotope ratio mass spectrometer, coupled to a Kiel I automated carbonate preparation device. All of these isotope records are shown in Extended Data Fig. 2, plotted against depth in core. The carbon isotope excursion seen in our record is 3.4‰, which is much higher than the benthic carbon isotope excursion (about 1.8‰) presented in ref. 41. This discrepancy arises because the earlier study[41] reports lower-resolution data, and did not take samples through the core interval of the CIE at Site 401 (202.55 to 202.41 metres composite depth (mcd)). However, we note that ref. 35 shows a very similar magnitude of change in $\delta^{13}C$ values to us; these $\delta^{13}C$ data, obtained from the same species (*M. subbotinae*), register a shift from 4.87‰ at 202.58 mcd to 1.47‰ at 202.46 mcd (an identical excursion magnitude of 3.4‰). The core containing the PETM (core 401-14) shows some rotary-drilling-induced deformation across the CIE. Such deformation commonly occurs across abrupt changes in lithology, but there is no obvious coring gap[35].

Effect of $\delta^{11}B$–pH calibration on pH excursion. Using the appropriate $\delta^{11}B$–pH calibration in order to convert calcite $\delta^{11}B$ into ambient seawater pH is essential for any palaeo-pH reconstruction. For late-Neogene studies using extant foraminifer species, the species used are typically calibrated for their $\delta^{11}B_{calcite}$-to-pH dependency using culture or field studies[42,43] in order to assess the magnitude of $\delta^{11}B$ vital effects that relate to foraminiferal physiology[44–46]. However, the species that we used here is extinct, making such calibrations impossible.

In order to bracket the likely magnitude of vital effects, and following ref. 21, we present two calibrations: one using the $\delta^{11}B$-to-pH relationship of aqueous borate[47], and the other using the *Trilobatus sacculifer* calibration[43]. We used the aqueous borate calibration for the pH trends shown in Figs 2 and 3, while Extended Data Fig. 3a presents the alternative outcome. As noted previously[20,46], when the pre-PETM pH is fixed (as is the case here), the choice of $\delta^{11}B$–pH calibration has little impact on the reconstructed pH curve. We note that the aqueous borate ion calibration is more conservative and is our preferred option, for the following reasons: first, not all modern species show a reduced sensitivity to pH relative to aqueous borate[48]; and second, previous studies have argued for a reduced magnitude of $\delta^{11}B$ vital effects in Eocene foraminifera.

$\delta^{18}O$- and Mg/Ca-based temperature reconstructions. *Morozovella subbotinae* inhabited the surface ocean mixed layer, and the temperatures used for determining pK_B^* (that is, the pH for which equal proportions of boric acid and borate ion are present in seawater; this value varies as a function of temperature, pressure and salinity) (see Extended Data Fig. 8) were obtained using the $\delta^{18}O_{calcite}$-to-temperature relationship of inorganic carbonates[49] and a local northwest Atlantic seawater $\delta^{18}O_{SMOW}$ (standard mean ocean water) reference value of 0.014‰ (ref. 50). The Mg/Ca-based temperatures shown in Extended Data Fig. 8 were calculated using deep-time foraminiferal Mg/Ca palaeothermometry[51], with the same parameters as ref. 2.

Determination of seawater $\delta^{11}B$. Boron in seawater has a residence time of somewhere between 11 million years and 20 million years (refs 52, 53), and so far $\delta^{11}B_{sw}$ has not been well constrained for the PETM. Thus, in order to create a self-consistent model–data set-up, we used the output of the GENIE Earth system model in the pre-CIE configuration, which, for the open northeast Atlantic, provides a pH of 7.75 (ref. 6). Using this pH information and the generic borate ion calibration[47] for the pH-dependent incorporation of boron into *M. subbotinae* resulted in a $\delta^{11}B_{sw}$ of 38.94‰ ± 0.41‰. The uncertainty in deriving this bulk seawater $\delta^{11}B$ is based on 10,000 realizations of a borate-ion-to-pH conversion with the commonly used, experimentally derived boron fractionation factor[47], varying the given $\delta^{11}B$ randomly within its 2σ measurement uncertainty, and also varying salinity by ±1.5 practical salinity units (psu) and temperature by ±1.5 °C. Using the *T. sacculifer* $\delta^{11}B$–pH calibration[43], but following the same approach, gives a $\delta^{11}B_{sw}$ of 37.6‰ ± 0.5‰.

Chronology for Site 401. We established a new and detailed age model for Site 401 by aligning our new, ultra-high-resolution (1 cm spacing) bulk carbonate $\delta^{18}O$ and $\delta^{13}C$ records with equivalent bulk carbonate isotope records from Site 690, using the Analyseries software[54]. Most stratigraphic correlation tie points (vertical lines in Extended Data Fig. 4) were made using the $\delta^{18}O$ records, which gave excellent agreement between the sites. The bulk $\delta^{18}O$ record from Site 401 shows high structural similarity to the $\delta^{18}O$ record of *M. subbotinae* from this site (Extended Data Fig. 2), and also to the $\delta^{18}O$ record of the thermocline-dwelling *Subbotina patagonica*[35], suggesting that bulk sediment $\delta^{18}O$ at Site 401 provides a reliable record of basic trends in upper-ocean warming and cooling across the PETM. A dominant control on the bulk $\delta^{18}O$ signal by temperature makes sense, given the scale of global surface ocean warming across the PETM[2] (4–5 °C). The fidelity of the bulk $\delta^{13}C$ record from Site 401 is likewise supported by its high structural similarity to the $\delta^{13}C$ record of *M. subbotinae* (Extended Data Fig. 2) and to the $\delta^{13}C$ record of *S. patagonica*[35]. It is also consistent with the bulk $\delta^{13}C$ record from another nearby location (the Forada section in northern Italy), which also shows an unusually early recovery to higher $\delta^{13}C$ values following an initial excursion to lowest values at PETM onset[55]. The Forada section is considered to be complete, because the CIE interval covers the maximum number of precession cycles[25]. There are at present two detailed age models for Site 690; thus, with detailed correlations to Site 401, we could transpose both the astronomically calibrated chronology[25,56] and an extraterrestrial helium-based chronology[57] onto Site 401. Extended Data Fig. 3b, c compares our pH record from Site 401 on both chronologies. Uncertainties relating to the choice of age model, and their impact on the calculated duration of the onset phase, have been evaluated via modelling sensitivity experiments (Extended Data Fig. 5) and have no impact on the findings discussed in the text.

A very different timescale for PETM carbon release during the CIE has been suggested[58], arguing that the PETM CIE had an onset of just 13 years. This proposal has proven controversial[59–63]; in particular, geochemical modelling constraints[59] and the discovery of drilling-induced disturbance of the core (creating the impression of annual layering) have cast substantial doubt on the suggestion. Indeed, further analysis of the carbon and oxygen isotope records using an Earth system model leads to an estimate of 4 kyr or longer for the onset of the PETM[64]. Given cyclostratigraphy-based age constraints for the duration of the PETM CIE[25] and a [3]He-based age model based on Ocean Drilling Program Site 690 (ref. 57), in addition to absolute and cyclostratigraphic age constraints from Spitsbergen[16], we regard as more plausible an age model that leads to a multimillennial CIE onset. However, as analysed (Extended Data Fig. 5) and discussed earlier, assumptions regarding the duration of the PETM onset interval itself are not essential to our conclusions.

Earth system modelling. *Configuration and data inversion.* cGENIE is an Earth system model of 'intermediate complexity'[65], comprising: a three-dimensional dynamic ocean circulation model with two-dimensional dynamic sea-ice non-dynamical atmosphere components[66]; a representation of the biogeochemical cycling of a variety of elements and isotopes in the ocean[67], including [13]C (ref. 68), plus representations of the preservation and burial of biogenic carbonates in accumulating marine sediments of the open ocean[68]; and terrestrial weathering[69,70]. We used cGENIE in the same early Eocene configuration as in refs 24 and 64, but with the terrestrial weathering feedback enabled.

We introduce three separate innovations to the model here. The first builds on previous work[7,71] that 'inverts' an observed $\delta^{13}C$ record to recover the underlying

time history of carbon release. In this, cGENIE adjusts mean atmospheric or surface ocean $\delta^{13}C$ to match a (proxy data) target at each model time-step (around one week). If the present mean model value lies above the data value (observed data are automatically linearly interpolated to the model time-step), a pulse of carbon is released to the atmosphere (or ocean). If the model value lies below the data value, then, depending on the experimental set-up, either carbon is removed from the atmosphere or nothing is done (see Fig. 3). The magnitude of the carbon pulse emitted at each time-step is prescribed and chosen such that the fastest observed change in $\delta^{13}C$ can be closely tracked, but without creating excessive overshoots in modelled $\delta^{13}C$. Here, we allow a maximum rate of carbon emissions to the atmosphere of 10 Pg per year, and hence a magnitude for an individual pulse of about 0.21 Pg, corresponding to an instantaneous increase in atmospheric p_{CO_2} pCO_2 of about 0.1 p.p.m.

We diverge from this earlier approach[7,71] in that, rather than using a record of $\delta^{13}C$ as our model target to assimilate, we instead use our reconstructed surface ocean pH data from Site 401. The methodology is inherently the same, but rather than comparing mean model and observed $\delta^{13}C$ at each time-step, we contrast (model and data) pH, diagnosing the carbon flux to the atmosphere that is required so that the surface pH in the model tracks the data. The model–data comparison is done on the basis of a mean global surface ocean pH value, calculated in cGENIE. This is because the existence of seasonality in pH in the model but not in the data results in artefacts in the diagnosed carbon emissions when using a single (Site 401) surface ocean grid point in cGENIE.

We justify in several ways the assumption that proxy-reconstructed surface ocean pH at Site 401 can be representative of the global mean. First, there is a relatively close degree of correspondence (visually) between the globally distributed pH records available (Fig. 2). Second, ocean surface pH, both today and during the Paleocene–Eocene, is relatively uniform in the model (and supported by observations and proxies, respectively), with maximum surface gradients between upwelling regions and subpolar regions of no more than 0.1 pH units today, and considerably less than this in the late Paleogene (probably mainly because of the nonlinear nature of the pH scale) (Extended Data Fig. 6). Third, these muted patterns are retained largely unaltered in response to CO_2 emissions. For instance, when we calculate the (annual mean) surface ocean pH anomaly at different times across the PETM (experiment number R07sm_Corg) as compared with the pre-PETM pattern, we find a generally uniform (to within ± 0.02 pH units) pattern in pH change (Extended Data Fig. 6). Last, if we contrast the evolution of global and annual mean surface ocean pH across the PETM (R07sm_Corg) with the (annual mean) surface pH at the location of Site 401 for the time points available (Extended Data Fig. 6, top), we also find that the pH at Site 401 is globally representative (and vice versa). All of this goes to illustrate that there is unlikely to be any substantive artefact in our assumption that our pH record at Site 401 can be treated as a surrogate for the global and annual mean in the model inversion experiment. For comparison, a similar analysis for the modern ocean under a future ocean acidification scenario (here, chosen to follow the representative concentration pathway (RCP) for carbon-dioxide emissions scenario 6.0; ref. 72) is shown in Extended Data Fig. 6 and demonstrates a comparably spatially uniform pattern of pH change.

Our second innovation involves determining the $\delta^{13}C$ values of the carbon emitted to the atmosphere. Previously[7,71], the $\delta^{13}C$ of the carbon was treated as an unknown, and a range of different possible values (and hence carbon sources and reservoirs) was tested in turn. However, given that observed pH constrains the magnitude of carbon emissions, we can now simultaneously use our observed $\delta^{13}C$ record to determine the source of carbon. The way in which the 'double inversion' methodology then works is that, for each model time-step, following the assessment of whether or not a pulse of carbon is emitted to the atmosphere (based on the model–data pH difference), model and observed Site 401 $\delta^{13}C$ values are compared. If the present mean model surface ocean $\delta^{13}C$ value lies above the present data value, then the carbon emitted is assigned a carbon isotopic value of $-100‰$. If, however, the mean model value lies below the data value, then a carbon isotopic value of $0‰$ is assigned. By binning the emission fluxes in time and calculating a flux-weighted average $\delta^{13}C$ (as in Fig. 3), intermediate $\delta^{13}C$ values (between $-100‰$ and $0‰$) are achieved. We emphasize that we are not assuming a source that could be $-100‰$ per se. This choice of extremely depleted value simply gives the model greater flexibility in tracking the trend in $\delta^{13}C$ emissions: isotopically intermediate mean annual carbon emissions arise by varying proportions of individual $0‰$ and $-100‰$ carbon pulses. We could have used any value as long as it is as least as light as the lightest potential source (for example, $-60‰$).

For our third innovation, in the situation in which the mean model surface ocean $\delta^{13}C$ value becomes lower than the observed Site 401 value, we test the importance of the burial of marine organic carbon (C_{org}). This works identically to the negative emissions diagnosed previously[7,71] (when carbon is removed from the system to force $\delta^{13}C$ to become more positive), but rather than prescribing the

$\delta^{13}C$ value, we calculate it according to a simple phytoplankton organic matter fractionation scheme[67,73].

For all of our experiments, we first spun up the model under late Palaeocene boundary conditions[24,64], here choosing an open-system run time of 200 kyr in order to fully bring the long-term $\delta^{13}C$ cycle into balance (and following on from an initially closed system spin-up of 20 kyr, used to established the basic climate and ocean circulation state). We then carried out a range of experiments (Extended Data Table 1a). We tested combinations (not all reported here) of: age model/orbital cyclostratigraphy ('R07') versus ^{3}He-based age modelling ('FE'); uncertainty in the pH reconstruction (mean (no additional identification tag) versus 2.5% and 97.5% confidence limits; 'LO' and 'HI', respectively); whether or not the data are smoothed ('sm') or raw ('rw'); whether or not climate-dependent weathering feedback was allowed (no additional identification tag), or weathering was fixed ('noW'); and whether or not C_{org} burial was enabled ('Corg' is appended to the run identification when carbon burial was enabled). These experiments were run for 500 kyr of simulation, with the exception of the carbon-burial Corg series (Extended Data Table 1a), which were run for an initial interval of 72.6 kyr (up until the peak of the CIE) with no organic carbon burial allowed, and then for a further 227.4 kyr with carbon burial allowed when needed (for a total of 300 kyr of simulation). Model results are plotted relative to the observed data point that defines PETM onset. *Additional sensitivity experiments and analysis.* We also carried out a range of sensitivity experiments to explore the importance (or otherwise) of the assumed duration of the CIE onset—in other words, whether there is a strong age model dependence of diagnosed total carbon emissions. In this series of experiments, the CIE onset phase was assumed to occur as a simultaneous linear decline in both $\delta^{13}C$ (by $-3.5‰$) and pH (by -0.3 pH units). We varied the duration of this decline from 100 to 20,000 years. Once the minima in $\delta^{13}C$ and pH were reached, these values were held constant up until the end of the experiment (a total of 50 kyr). The same double-inversion methodology was used as in the main experiments, starting from the same spin-up state (Extended Data Fig. 5 and Extended Data Table 1b).

For further details of the model and its configuration, as well as a comprehensive discussion of the model uncertainties, see Supplementary Information. See Extended Data Fig. 7 for an assessment of the evolution of the model-projected global mean, and Extended Data Fig. 8 for spatial patterns of sedimentary wt% calcium carbonate and sea surface temperature (also described in Supplementary Information). Site-specific model–data comparisons are shown in Extended Data Fig. 9 (and again discussed in full in Supplementary Information).

Model code and availability of supporting files. The source code of the cGENIE Earth system model used here—together with specific experimental configurations, boundary conditions, and data-forcing files—is available for download. A brief description of obtaining the code, configuring cGENIE, and executing and analysing the published model experiments is available at http://www.seao2.info/cgenie/pubs/gutjahretal.2017.txt. Further specific details of, for example, processing the model results, the configurations of the experiments shown in Extended Data or in Supplementary Information, or the raw model output, are available and can be obtained directly from A.R. (andy@seao2.org).

Data availability. Foraminifera and bulk carbonate stable-isotope results can be found in Supplementary Information and accessed through the UK National Geoscience Data Centre (http://www.bgs.ac.uk/services/ngdc/). All modelling-related data are included as part of the cGENIE model code distribution (see above).

34. Pardo, A., Keller, G., Molina, E. & Canudo, J. I. Planktic foraminiferal turnover across the Paleocene–Eocene transition at DSDP site 401, Bay of Biscay, North Atlantic. *Mar. Micropaleontol.* **29,** 129–158 (1997).
35. Bornemann, A. *et al.* Persistent environmental change after the Paleocene–Eocene Thermal Maximum in the eastern North Atlantic. *Earth Planet. Sci. Lett.* **394,** 70–81 (2014).
36. Sexton, P. F., Wilson, P. A. & Pearson, P. N. Microstructural and geochemical perspectives on planktic foraminiferal preservation: "glassy" versus "frosty". *Geochem. Geophys. Geosyst.* **7,** Q12P19 (2006).
37. Foster, G. L. Seawater pH, pCO$_2$ and [CO$_3^{2-}$] variations in the Caribbean Sea over the last 130 kyr: a boron isotope and B/Ca study of planktic forminifera. *Earth Planet. Sci. Lett.* **271,** 254–266 (2008).
38. Foster, G. L. *et al.* Interlaboratory comparison of boron isotope analyses of boric acid, seawater and marine CaCO$_3$ by MC-ICPMS and NTIMS. *Chem. Geol.* **358,** 1–14 (2013).
39. Barker, S., Greaves, M. & Elderfield, H. A study of cleaning procedures used for foraminiferal Mg/Ca paleothermometry. *Geochem. Geophys. Geosyst.* **4,** 8407 (2003).
40. Henehan, M. J. *et al.* Calibration of the boron isotope proxy in the planktonic foraminifera *Globigerinoides ruber* for use in palaeo-CO$_2$ reconstruction. *Earth Planet. Sci. Lett.* **364,** 111–122 (2013).
41. Nunes, F. & Norris, R. D. Abrupt reversal in ocean overturning during the Palaeocene/Eocene warm period. *Nature* **439,** 60–63 (2006).

42. Sanyal, A., Bijma, J., Spero, H. & Lea, D. W. Empirical relationship between pH and the boron isotopic composition of *Globigerinoides sacculifer*: implications for the boron isotope paleo-pH proxy. *Paleoceanography* **16**, 515–519 (2001).

43. Martínez-Botí, M. A. *et al.* Boron isotope evidence for oceanic carbon dioxide leakage during the last deglaciation. *Nature* **518**, 219–222 (2015).

44. Zeebe, R. E., Wolf-Gladrow, D. A., Bijma, J. & Hönisch, B. Vital effects in foraminifera do not compromise the use of delta B-11 as a paleo-pH indicator: evidence from modeling. *Paleoceanography* **18**, 1043 (2003).

45. Hönisch, B. *et al.* The influence of symbiont photosynthesis on the boron isotopic composition of foraminifera shells. *Mar. Micropaleontol.* **49**, 87–96 (2003).

46. Foster, G. L. & Rae, J. W. B. Reconstructing ocean pH with boron isotopes in foraminifera. *Annu. Rev. Earth Planet. Sci.* **44**, 207–237 (2016).

47. Klochko, K., Kaufman, A. J., Yao, W. S., Byrne, R. H. & Tossell, J. A. Experimental measurement of boron isotope fractionation in seawater. *Earth Planet. Sci. Lett.* **248**, 276–285 (2006).

48. Henehan, M. J. *et al.* A new boron isotope-pH calibration for *Orbulina universa*, with implications for understanding and accounting for 'vital effects'. *Earth Planet. Sci. Lett.* **454**, 282–292 (2016).

49. Kim, S.-T. & O'Neil, J. R. Equilibrium and nonequilibrium oxygen isotope effects in synthetic carbonates. *Geochim. Cosmochim. Acta* **61**, 3461–3475 (1997).

50. Tindall, J. *et al.* Modelling the oxygen isotope distribution of ancient seawater using a coupled ocean-atmosphere GCM: implications for reconstructing early Eocene climate. *Earth Planet. Sci. Lett.* **292**, 265–273 (2010).

51. Evans, D. & Müller, W. Deep time foraminifera Mg/Ca paleothermometry: nonlinear correction for secular change in seawater Mg/Ca. *Paleoceanography* **27**, PA4205 (2012).

52. Spivack, A. J. & Edmond, J. M. Boron isotope exchange between seawater and the oceanic crust. *Geochim. Cosmochim. Acta* **51**, 1033–1043 (1987).

53. Lemarchand, D., Gaillardet, J., Lewin, E. & Allegre, C. J. Boron isotope systematics in large rivers: implications for the marine boron budget and paleo-pH reconstruction over the Cenozoic. *Chem. Geol.* **190**, 123–140 (2002).

54. Paillard, D., Labeyrie, L. & Yiou, P. Macintosh program performs time-series analysis. *EOS* **77**, 379 (1996).

55. Giusberti, L. *et al.* Mode and tempo of the Paleocene–Eocene thermal maximum in an expanded section from the Venetian pre-Alps. *Geol. Soc. Am. Bull.* **119**, 391–412 (2007).

56. Röhl, U., Bralower, T. J., Norris, R. D. & Wefer, G. New chronology for the late Paleocene thermal maximum and its environmental implications. *Geology* **28**, 927–930 (2000).

57. Farley, K. A. & Eltgroth, S. F. An alternative age model for the Paleocene–Eocene Thermal Maximum using extraterrestrial He-3. *Earth Planet. Sci. Lett.* **208**, 135–148 (2003).

58. Wright, J. D. & Schaller, M. F. Evidence for a rapid release of carbon at the Paleocene–Eocene thermal maximum. *Proc. Natl Acad. Sci. USA* **110**, 15908–15913 (2013).

59. Zeebe, R. E., Dickens, G. R., Ridgwell, A., Sluijs, A. & Thomas, E. Onset of carbon isotope excursion at the Paleocene–Eocene thermal maximum took millennia, not 13 years. *Proc. Natl Acad. Sci. USA* **111**, E1062–E1063 (2014).

60. Pearson, P. N. & Nicholas, C. J. Layering in the Paleocene/Eocene boundary of the Millville core is drilling disturbance. *Proc. Natl Acad. Sci. USA* **111**, E1064–E1065 (2014).

61. Stassen, P., Speijer, R. P. & Thomas, E. Unsettled puzzle of the Marlboro clays. *Proc. Natl Acad. Sci. USA* **111**, E1066–E1067 (2014).

62. Wright, J. D. & Schaller, M. F. Reply to Pearson and Nicholas, Stassen et al., and Zeebe et al.: Teasing out the missing piece of the PETM puzzle. *Proc. Natl Acad. Sci. USA* **111**, E1068–E1071 (2014).

63. Pearson, P. N. & Thomas, E. Drilling disturbance and constraints on the onset of the Paleocene–Eocene boundary carbon isotope excursion in New Jersey. *Clim. Past* **11**, 95–104 (2015).

64. Zeebe, R. E., Ridgwell, A. & Zachos, J. C. Anthropogenic carbon release rate unprecedented during the past 66 million years. *Nat. Geosci.* **9**, 325–329 (2016).

65. Brady, P. V. The effect of silicate weathering on global temperature and atmospheric CO_2. *J. Geophys. Res.* **96**, 18101–18106 (1991).

66. Edwards, N. R. & Marsh, R. Uncertainties due to transport-parameter sensitivity in an efficient 3-D ocean-climate model. *Clim. Dyn.* **24**, 415–433 (2005).

67. Ridgwell, A. *et al.* Marine geochemical data assimilation in an efficient Earth system model of global biogeochemical cycling. *Biogeosciences* **4**, 87–104 (2007).

68. Ridgwell, A. & Hargreaves, J. C. Regulation of atmospheric CO2 by deep-sea sediments in an Earth system model. *Global Biogeochem. Cycles* **21**, GB2008 (2007).

69. Colbourn, G., Ridgwell, A. & Lenton, T. M. The time scale of the silicate weathering negative feedback on atmospheric CO_2. *Glob. Biogeochem. Cycles* **29**, 583–596 (2015).

70. Lord, N. S., Ridgwell, A., Thorne, M. C. & Lunt, D. J. An impulse response function for the 'long tail' of excess atmospheric CO2 in an Earth system model. *Global Biogeochem. Cycles* **30**, 2–17 (2016).

71. Cui, Y. & Kump, L. R. Global warming and the end-Permian extinction event: proxy and modeling perspectives. *Earth Sci. Rev.* **149**, 5–22 (2015).

72. IPCC. *Climate Change 2013: The Physical Science Basis. Contribution of Working Group I to the Fifth Assessment Report of the Intergovernmental Panel on Climate Change* (eds Stocker, T. F. *et al.*) (Cambridge Univ. Press, 2013).

73. Ridgwell, A. *Glacial–Interglacial Perturbations in the Global Carbon Cycle.* PhD thesis, Univ. East Anglia (2001).

74. Cao, L. *et al.* The role of ocean transport in the uptake of anthropogenic CO2. *Biogeosciences* **6**, 375–390 (2009).
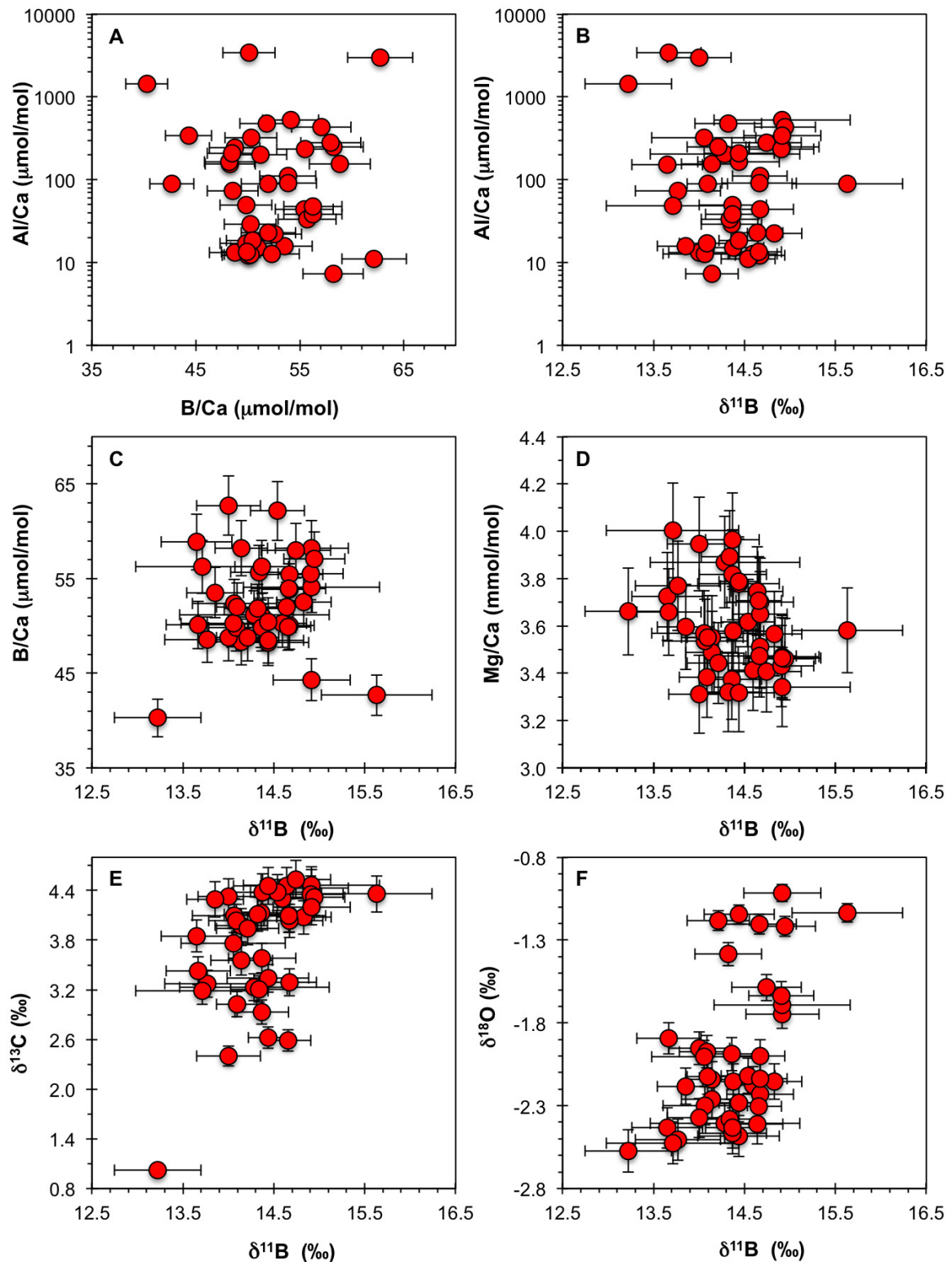
Extended Data Figure 1 | Elemental and stable-isotope cross-plots for *M. subbotinae*. a–f, We screened samples for chemical consistency by checking various elemental ratios (Al/Ca, B/Ca and Mg/Ca) as well as measured δ^{11}B and δ^{13}C.
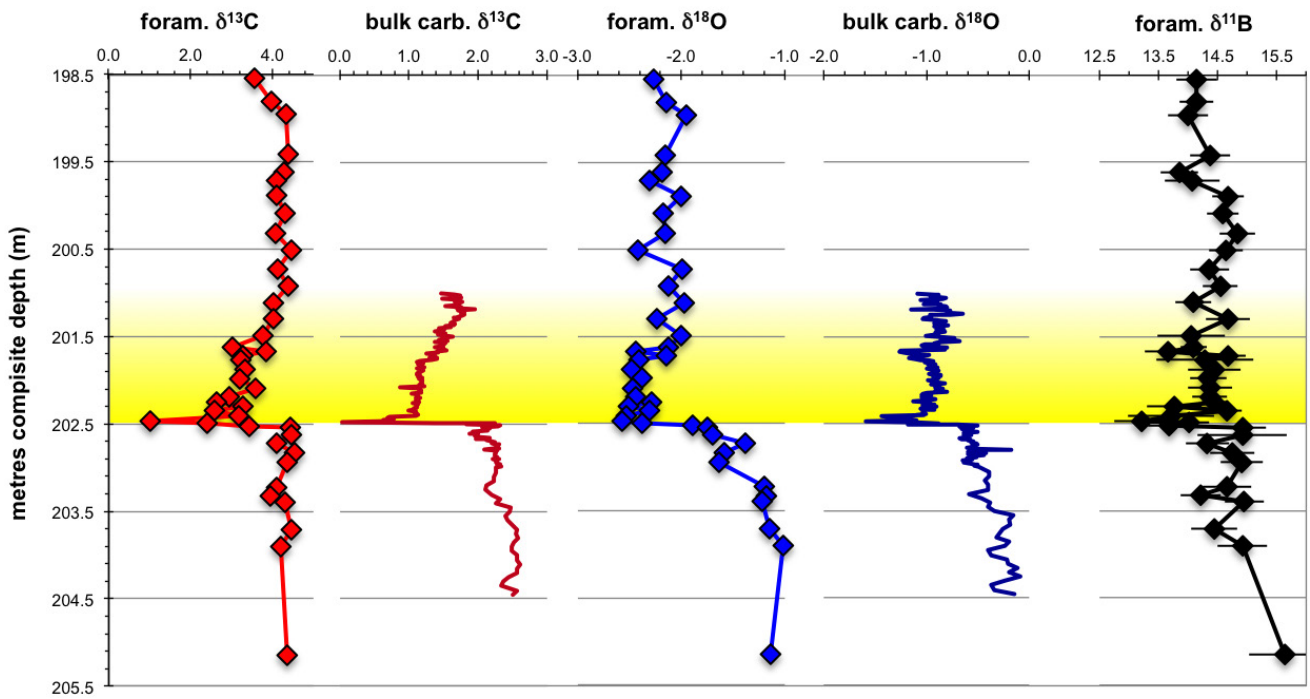
Extended Data Figure 2 | Stable-isotope data for foraminifera and bulk carbonate. Foraminifera-based stable-isotope compositions were generated from identical samples after splitting the $\delta^{13}C/\delta^{18}O$ fraction from the $\delta^{11}B$ fraction. For both foraminifera and bulk carbonate, the data are plotted against the depth of the core sample. The same data are plotted against age relative to CIE in Fig. 1.
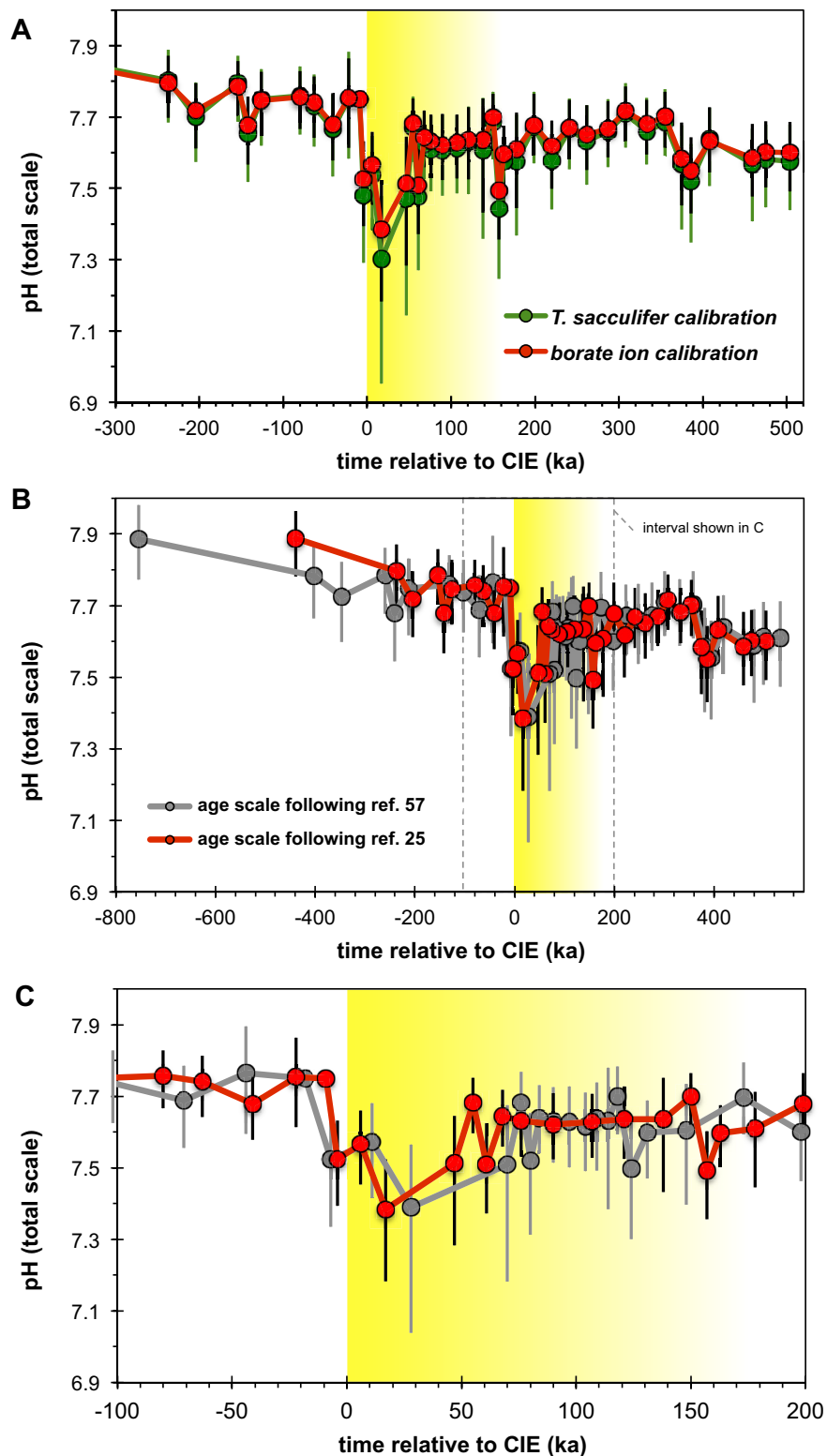
Extended Data Figure 3 | Illustration of the results of δ¹¹B-to-pH conversion, and differences in age models. a, We used our δ¹¹B measurements as a proxy to calculate the evolution of pH at Site 401 during the PETM CIE, using either the borate ion[47] (red) or the *T. sacculifer*[43] (green) calibration. The age scale used follows ref. 25. **b**, Direct comparison of our two age models, plotting the reconstructed pH evolution of Site 401 using either the age model of ref. 57 or our preferred age model[25]. **c**, Expanded view of **b**.
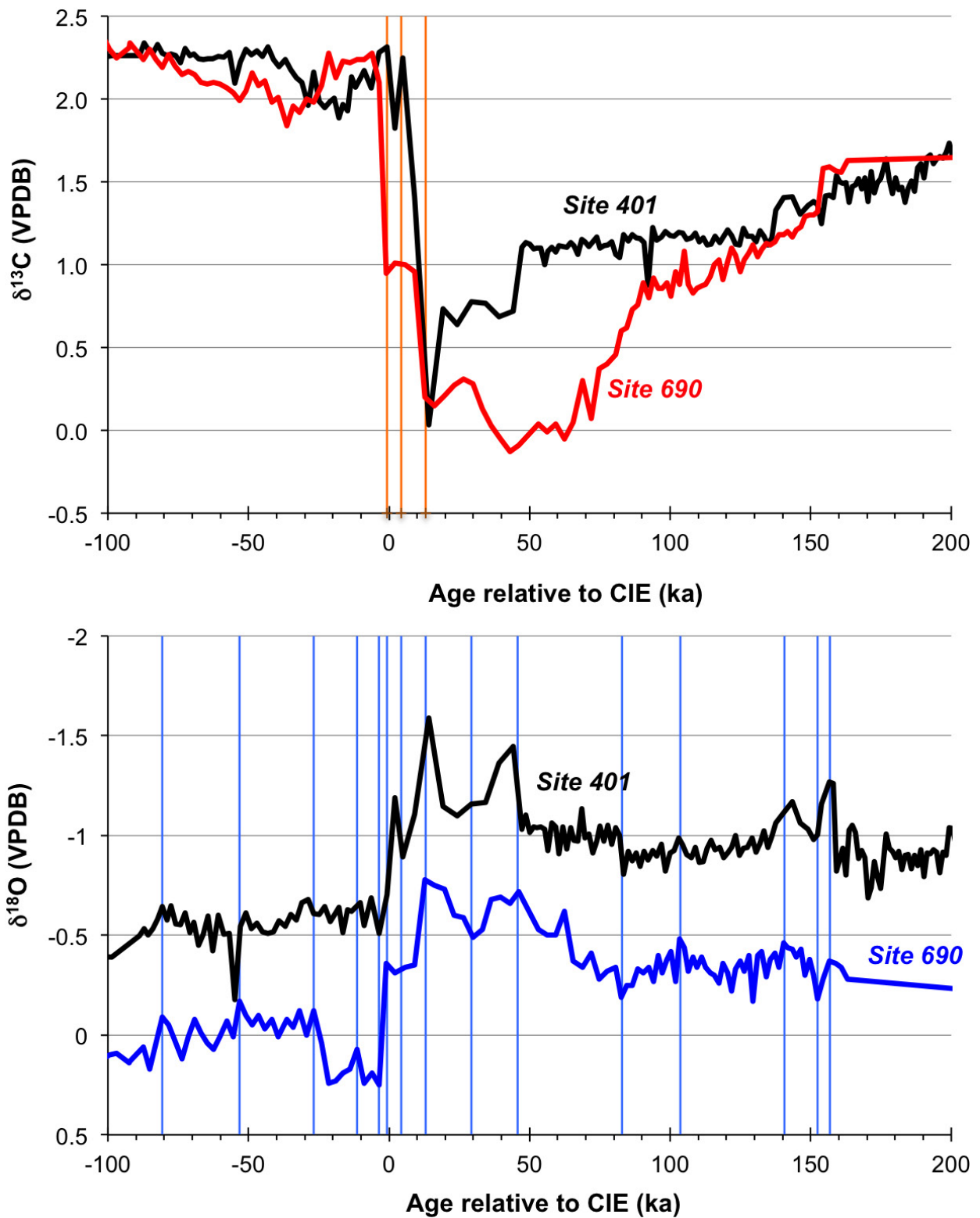
Extended Data Figure 4 | Selection of age-model tie points. Comparison of bulk carbonate δ^{13}C (top) and δ^{18}O (bottom) values for Site 401 and Site 690 (ref. 25). Vertical lines show the age tie points used to derive the age model relative to the PETM CIE (see Methods).
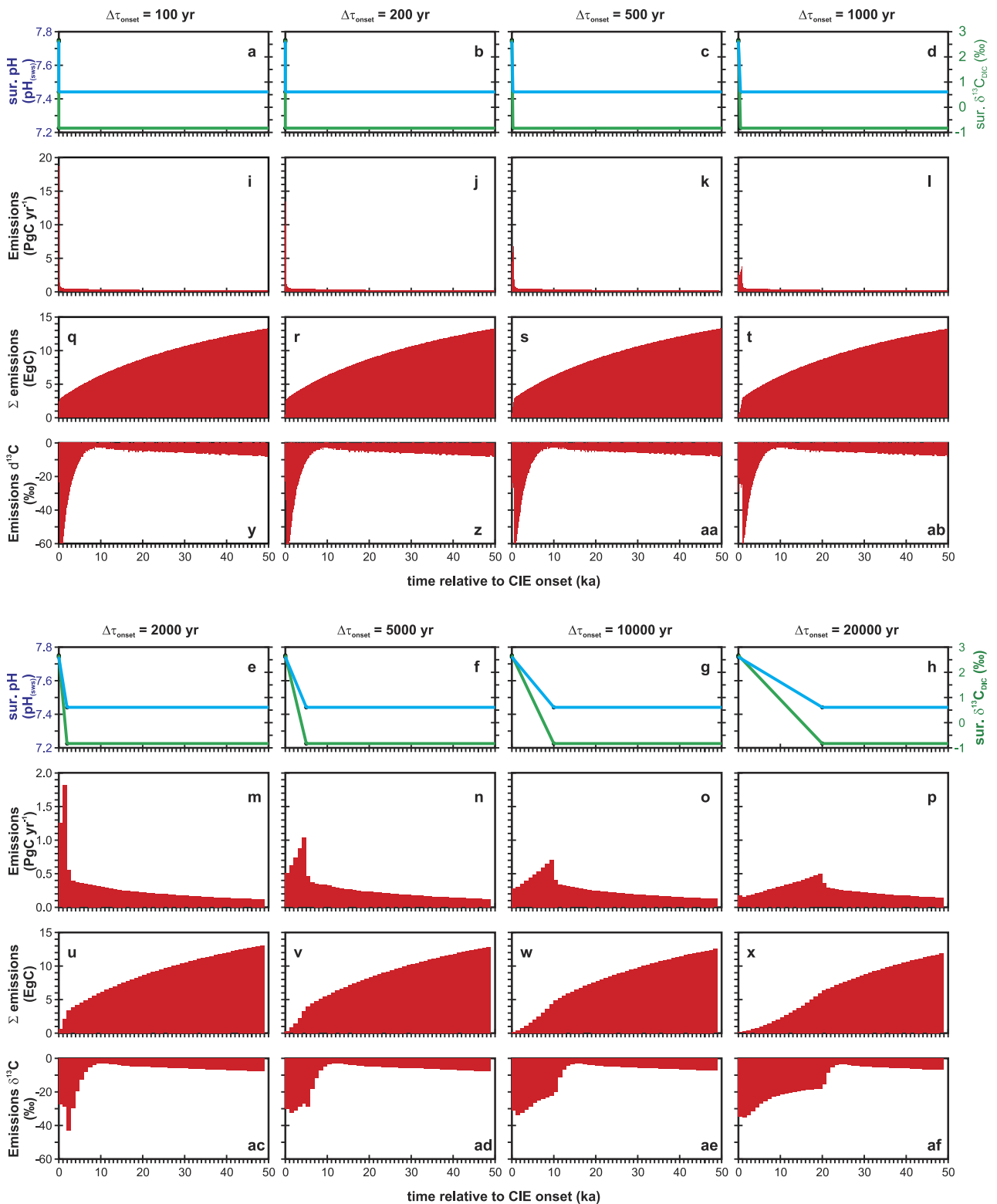
Extended Data Figure 5 | Key results of sensitivity experiments. The figure shows the influence of uncertainties in the CIE onset duration on diagnosed total carbon release. For these idealized experiments, the CIE onset phase was assumed to occur linearly, with the decline in ocean surface dissolved inorganic carbon (DIC) $\delta^{13}C$ (by 3.5‰) and pH (by 0.3 pH units) having a duration ($\Delta\tau_{onset}$) that varied from 100 to 20,000 years; thereafter, the target pH and $\delta^{13}C$ values were held constant until the end of the experiment (at 50,000 years). **a–h**, The evolution with time of these target ocean surface variables, with pH on the left-hand y axis, and $\delta^{13}C_{(DIC)}$ on the right-hand axis. **i–p**, Maximum carbon emission rate per time interval. **q–x**, Cumulative carbon emission per time interval in Eg of carbon. **y, z, aa–af**, Average emitted $\delta^{13}C$ per time interval.
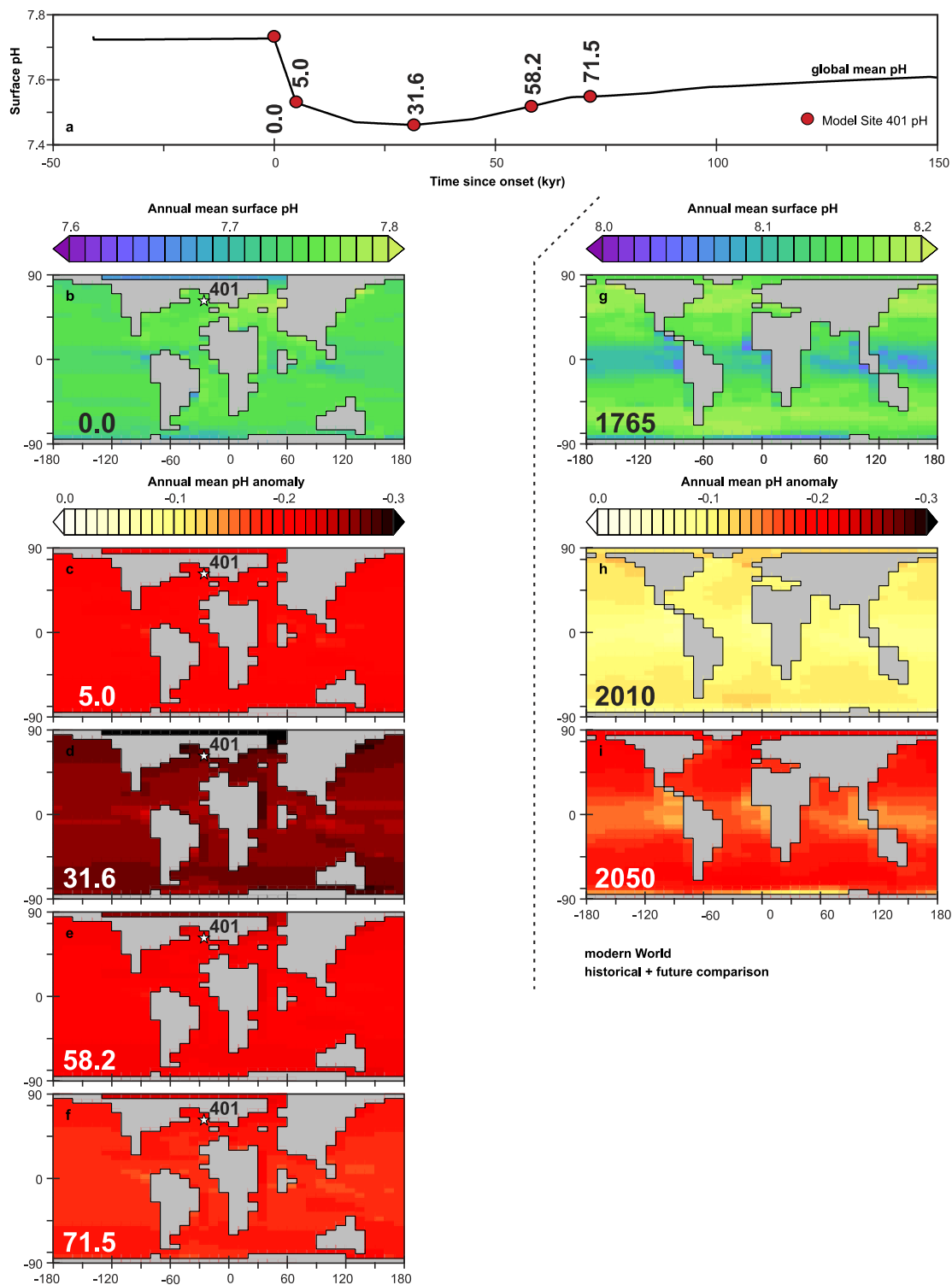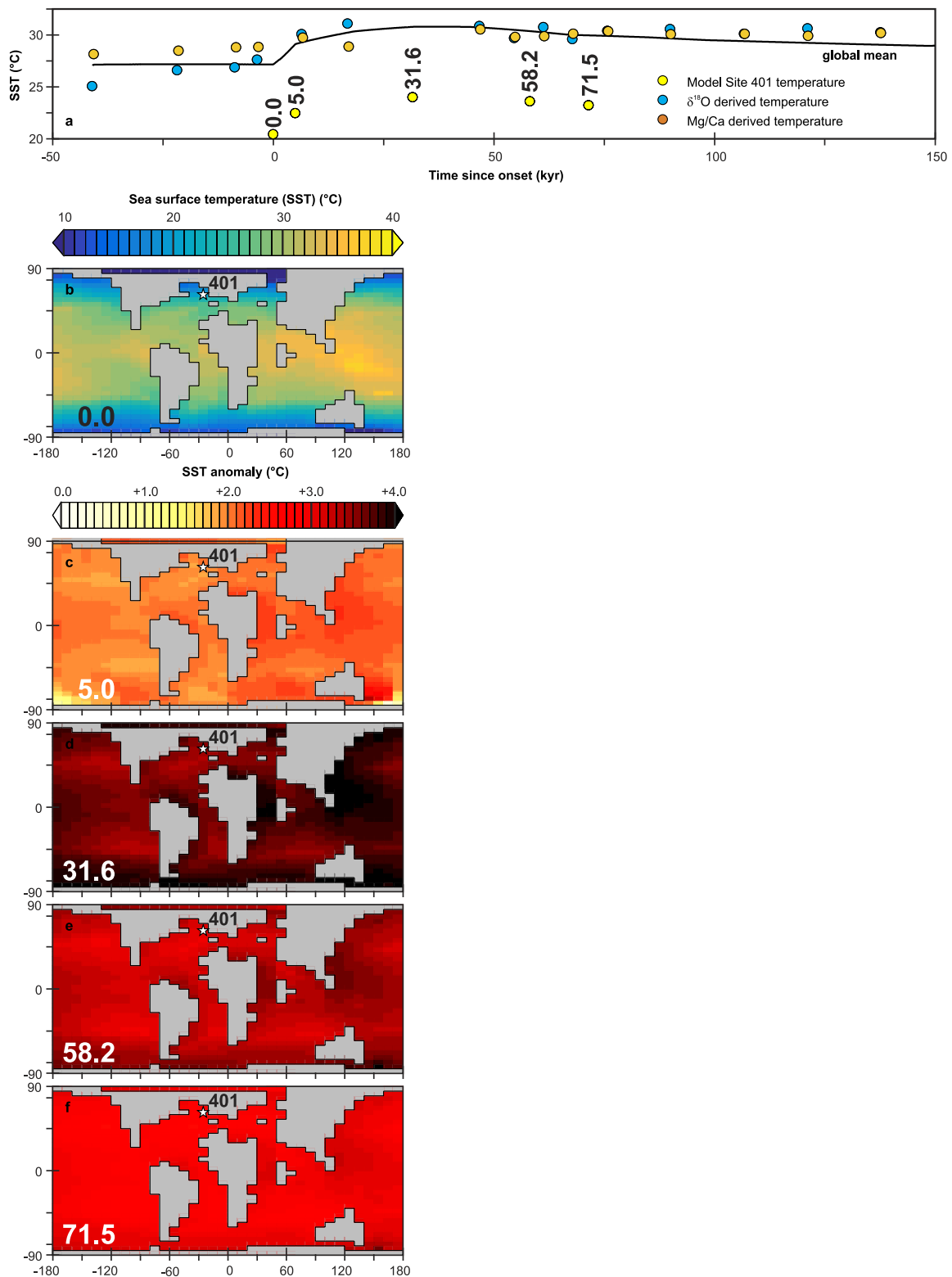
Extended Data Figure 6 | Spatial and temporal evolution of mean annual surface ocean pH in the Earth system model cGENIE, shown both for the PETM and for preindustrial and future times. a, Black line, global mean surface ocean pH values across the PETM, from experiment R07sm_Corg (these are our main pH estimates, obtained using the inorganic borate ion calibration and the RH07 age model, and including an assumption of organic carbon burial after the peak PETM). Red circles represent the annual mean pH values at Site 401 (location shown in **b**) in the model, taken at times in the model simulation that have corresponding δ^{11}B-derived pH data points (see Fig. 3b; note that we do not use all of the observed data points). **b**, Model-projected spatial pattern of annual mean surface ocean pH at time zero (that is, PETM onset). The star shows the location of Site 401. **c–f**, Model-projected spatial patterns of the annual mean surface ocean pH anomaly compared with time 0, for the highlighted time points from **a** (5.0, 31.6, 58.2 and 71.5 kyr after onset). **g**, Model-projected spatial pattern of annual mean surface ocean pH in the modern ocean under pre-industrial (year 1765) atmospheric CO_2 levels (278 p.p.m.). The model is configured as described in ref. 74 and driven with a CO_2 emissions scenario that is consistent with RCP 6.0. **h**, **i**, Model-projected spatial pattern of the annual mean surface ocean pH anomaly compared with that for 1765, at years 2010 and 2050. The scale is as for **c–f**.
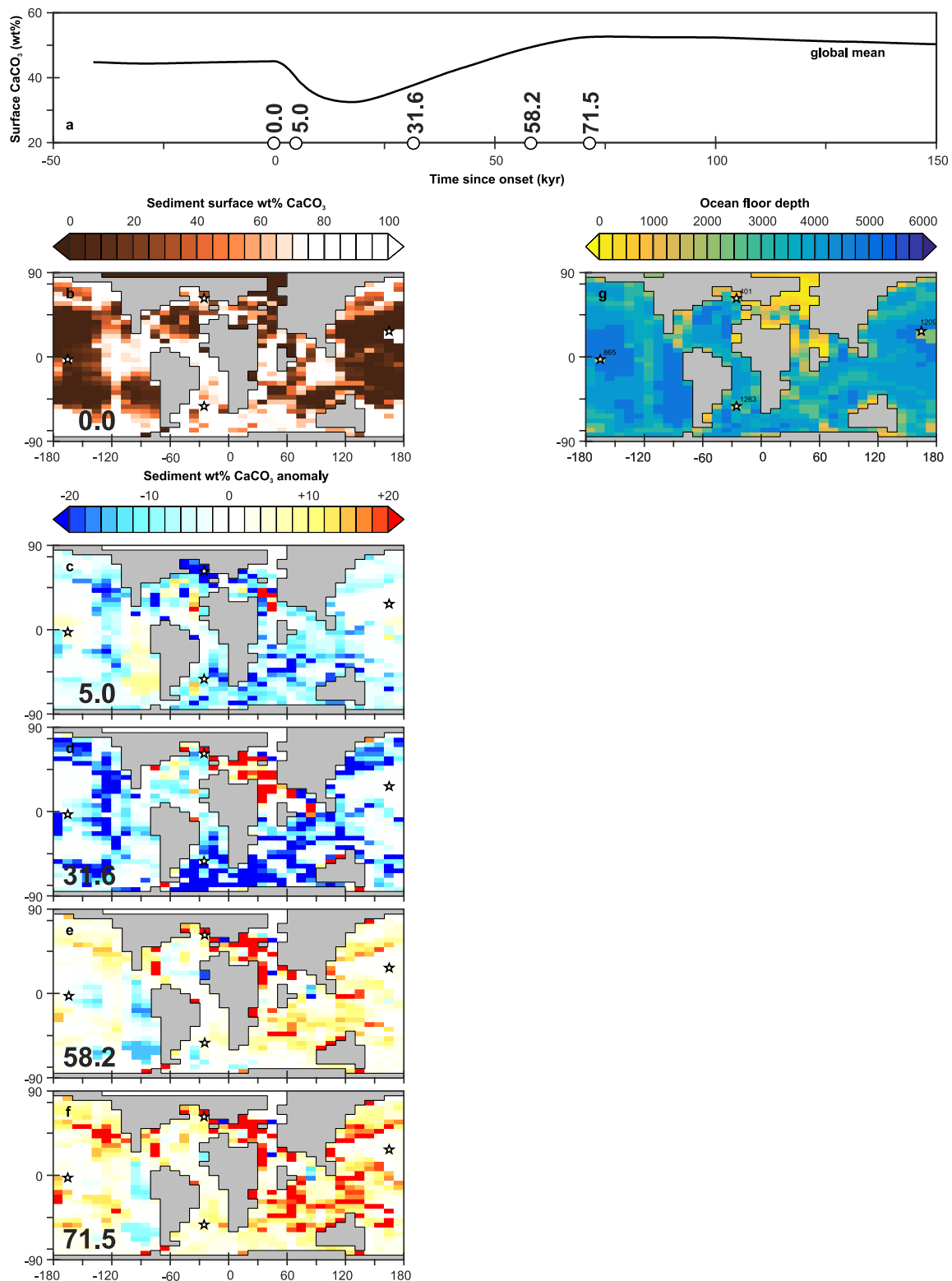
Extended Data Figure 7 | Spatial and temporal evolution of surface sedimentary calcium carbonate content in cGENIE during the PETM.
a, Black line, global mean surface levels (in wt%) of sedimentary calcium carbonate (CaCO$_3$) across the PETM, from experiment R07sm_Corg. White circles, times from PETM onset onwards that correspond to the δ^{11}B-derived pH data points in Fig. 3b and Extended Data Fig. 6. The white circles do not represent 'values', and simply mark specific time points. **b**, Model-projected spatial pattern of surface sedimentary wt% CaCO$_3$ at

time zero (PETM onset). Shown are the locations of sites for which surface ocean pH has been reconstructed (see Fig. 2) and at which detailed down-core model–data comparison is carried out (Extended Data Fig. 9). **c–f**, Model-projected spatial patterns of the surface sedimentary wt% CaCO$_3$ anomaly compared with time 0, for the time points highlighted in **a**. **g**, For reference, the assumed seafloor bathymetry in the model (and the locations of the four data-rich sites that are discussed in Supplementary Information).

Extended Data Figure 8 | Spatial and temporal evolution of sea surface temperature in cGENIE during the PETM. a, Black line, global and annual mean SSTs during the PETM, from experiment R07sm_Corg. Yellow circles, annual mean SST values at Site 401 in the model, at the times from PETM onset onwards that correspond to the δ^{11}B-derived pH data points (see Fig. 3b). Blue and orange circles, δ^{18}O- and Mg/Ca-derived SST estimates, respectively. **b**, Model-projected spatial pattern of annual mean SSTs at time 0. The star shows the location of Site 401. **c–f**, Model-projected spatial patterns of the annual mean SST anomaly compared with time 0, for the time points shown in **a**.

LETTER RESEARCH
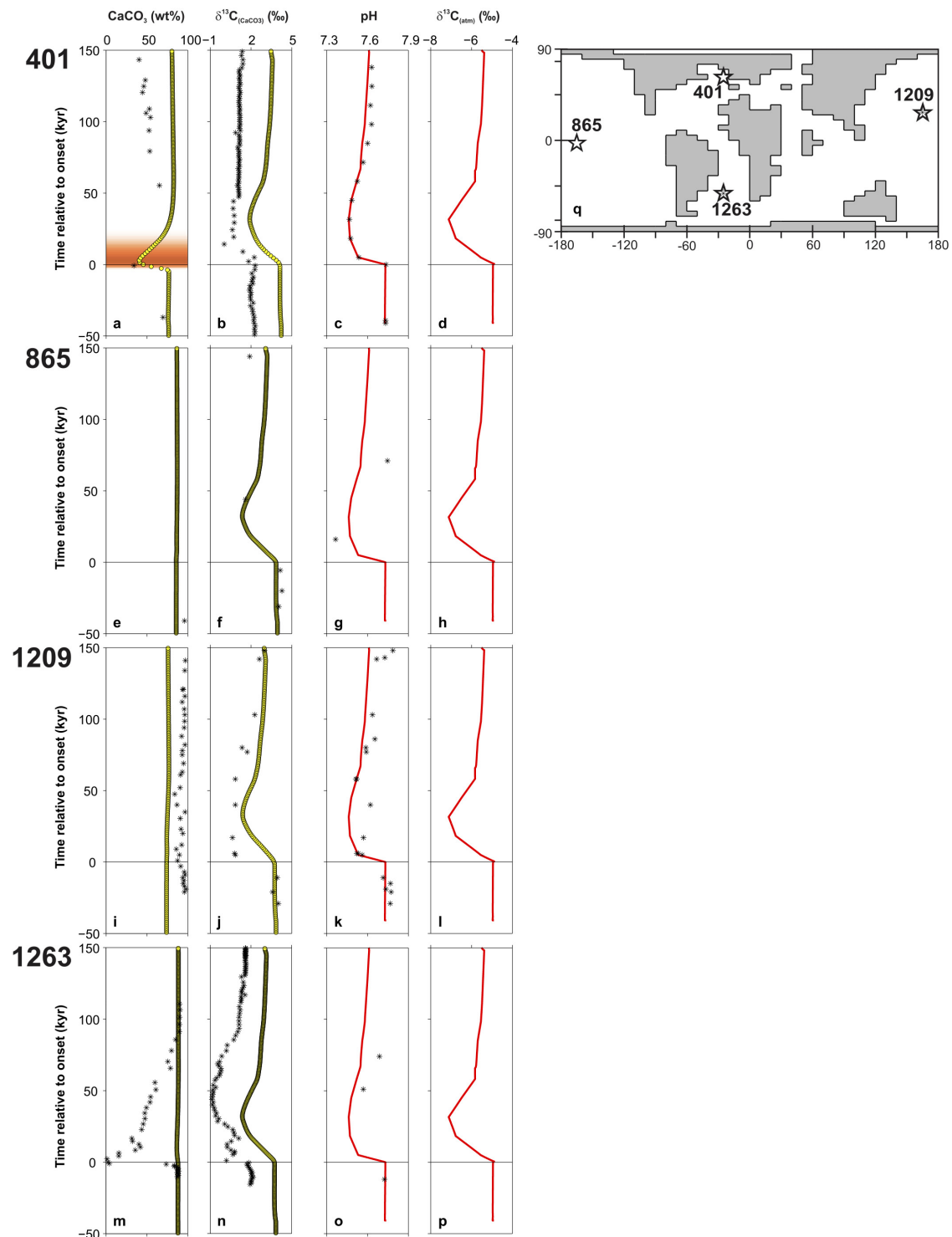
Extended Data Figure 9 | Down-core model–data evaluation at four data-rich sites. a–p, Comparisons for four Ocean Drilling Program Sites (401, 865, 1,209 and 1,263) for which surface ocean pH has been reconstructed across the PETM (Fig. 2; this study and ref. 20). **q,** The palaeo-locations of these sites in the cGENIE Earth system model. **a–p,** Model–data comparisons are made for: wt% CaCO$_3$ (**a, e, i, m**); δ^{13}C values from bulk carbonate (**b, f, j, n**); and surface ocean pH (**c, g, k, o**). Panels **d**, **h**, **l** and **p** provide an orientation in time, showing the projected evolution of atmospheric δ^{13}C from CO$_2$ in the model. For wt% CaCO$_3$ and δ^{13}C of bulk carbonate, model points (resolved at 1-cm intervals) are plotted as filled yellow circles. Model-projected pH values (global and

annual means, as in Fig. 3h and Extended Data Fig. 6a) and atmospheric δ^{13}C values for CO$_2$ are shown as continuous red lines. In all cases, observed data values are shown as asterisks. For Sites 865, 1,209 and 1,263, the age models—employing the original relative age-model constraints[20] used to convert from model-simulated sediment depths (resolved at 1-cm intervals) at each location in cGENIE—were calculated using a constant detrital flux accumulation rate. The observed data are plotted on the respective Site-690-derived age models[25]. Both model-based and data-based age scales are synchronized to time 0 (PETM onset; horizontal line). See Supplementary Information for details.

© 2017 Macmillan Publishers Limited, part of Springer Nature. All rights reserved.

Extended Data Table 1 | Key results from individual model runs

a

Experiment ID	experimental assumptions					peak emissions	cumulative emissions		cumulative C_org burial		ΔSST	peak excess weathering
	age model	δ¹¹B envelope	smoothed data?	weathering?	Corg burial?	(PgC yr⁻¹)	total (PgC)	mean δ¹³C (‰)	total (PgC)	mean δ¹³C (‰)	(°C)	(PgC yr⁻¹)
R07sm_HI	R07	high	YES	YES	NO	0.41	5,688	-18.9	---	---	2.25	0.030
R07sm	R07	mean	YES	YES	NO	0.58	10,213	-11.1	---	---	3.64	0.053
R07sm_LO	R07	low	YES	YES	NO	1.16	19,964	-6.6	---	---	5.99	0.105
FEsm_HI	FE	high	YES	YES	NO	0.17	6,502	-16.5	---	---	2.10	0.038
FEsm	FE	mean	YES	YES	NO	0.36	12,020	-9.8	---	---	3.09	0.069
FEsm_LO	FE	low	YES	YES	NO	0.64	24,124	-6.0	---	---	4.80	0.132
R07rw	R07	mean	NO	YES	NO	0.61	10,984	-12.1	---	---	4.07	0.061
FErw	FE	mean	NO	YES	NO	0.45	12,749	-10.2	---	---	3.14	0.072
R07sm_noW	R07	mean	YES	NO	NO	0.52	6,407	-16.7	---	---	3.34	---
FEsm_noW	FE	mean	YES	NO	NO	0.30	6,665	-16.4	---	---	2.72	---
R07sm_HI_Corg	R07	high	YES	YES	YES	0.41	7,670	-18.0	2,607	-30.0	2.25	0.030
R07sm_Corg	R07	mean	YES	YES	YES	0.58	12,220	-10.9	2,540	-30.5	3.64	0.053
R07sm_LO_Corg	R07	low	YES	YES	YES	1.16	22,593	-7.1	3,333	-30.9	5.99	0.105

b

Duration of onset (yr)	peak emissions (PgC yr⁻¹)	cumulative emissions over onset		cumulative emissions @ 20,000 yr		cumulative emissions @ 50,000 yr	
		total (PgC)	mean δ¹³C (‰)	total (PgC)	mean δ¹³C (‰)	total (PgC)	mean δ¹³C (‰)
100	20.00	1,897	-19.0	8,695	-17.0	13,256	-13.4
200	15.21	2,355	-18.4	8,688	-17.0	13,252	-13.4
500	6.90	2,588	-21.5	8,664	-17.0	13,239	-13.6
1,000	3.72	2,799	-24.5	8,613	-17.1	13,200	-13.4
2,000	2.08	3,074	-27.6	8,526	-17.2	13,181	-13.4
5,000	1.07	3,751	-29.0	8,202	-17.8	13,007	-13.5
10,000	0.70	4,691	-26.3	7,612	-18.8	12,706	-13.6
20,000	0.48	6,141	-22.0	6,141	-22.0	12,025	-14.0

a, Summary of the main double-inversion experiments carried out. In the experiment identification (ID) column, R07 refers to configurations that tie the Site 401 records to the chronostratigraphy of ref. 25; FE refers to the ³He-based age model of ref. 57; sm refers to the inversion of analytically smoothed δ¹³C and pH data sets; rw denotes usage of original sample data for double inversions; HI and LO represent potentially extreme configurations that take into account the boron-proxy uncertainty at the 95% confidence level; noW refers to the disabling of silicate (and carbonate) weathering feedbacks; Corg refers to model configurations that allow the removal of excess organic carbon from the surface ocean. Grey shading highlights experiments that are discussed in the text and plotted in Fig. 3. Note that, first, peak emissions are binned at 2-kyr intervals; second, both cumulative emissions and C_org (organic carbon) burial are measured from 40,000 years ago to 190,000 years ago (model time); and third, peak excess weathering reflects carbon removal owing to silicate weathering above pre-PETM weathering rates.
b, Summary table presenting the results of sensitivity experiments (shown in Extended Data Fig. 5) to quantify the importance of uncertainties in the age model for the CIE onset. In these experiments, the CIE onset phase is assumed to occur linearly, with the decline in δ¹³C and pH varying with a duration of 100 to 20,000 years. Shown are: diagnosed peak carbon emissions; cumulative carbon emissions occurring over the duration of the onset, and mean (flux-weighted) δ¹³C values for these emissions; cumulative carbon emissions occurring at the 20,000-year time horizon (comparable to the onset duration in our assumed age model), and mean (flux-weighted) δ¹³C values for these emissions; and cumulative carbon emissions occurring at the 50,000-year horizon, plus the mean (flux-weighted) δ¹³C values for these emissions. Note that in all experiments, once the onset is complete, the target pH and δ¹³C values are held constant (and low) until the end of the xperiment (50,000 years).